Design of

Precision Kinematic Systems

Dipl.-Ing. Philipp Schmiechen

Submitted to the Department of Mechanical Engineering

in Partial Fulfillment of the Requirements for the Degree of

Master of Science in Mechanical Engineering

at the

Massachusetts Institute of Technology

December 1992

Signature of Author _____
Department of Mechanical Engineering
December 18, 1992

Certified by _____
Alexander H. Slocum
Associate Professor of Mechanical Engineering
Thesis Supervisor

Accepted by _____
Professor Ain A. Sonin
Chairman, Graduate Committee

Design of

Precision Kinematic Systems

Dipl.-Ing. Philipp Schmiechen

Summary

The ever increasing demand for higher accuracy and repeatability requires the designer to reconsider and reevaluate his methods. As one means to design for high accuracy, this thesis explores the potential of kinematic design. Kinematic design seeks to predict the accuracy of a design by generating a family of unique solutions. This contrasts the principle of elastic averaging, where a manifold of solutions exists. From the very beginning of the design process kinematic design enables the designer to obtain good estimates of a design's achievable performance.

The advantages of a kinematic approach for many design problems have been shown and examples are provided herein for a zero degree of freedom system and a one degree of freedom system. The necessary steps of the design analysis are presented and with today's computational tools, the design of precision fixturings and motion systems following the kinematic design paradigm can become a straightforward matter.

Thesis Supervisor: Dr. Alexander H. Slocum

Title: Associate Professor of Mechanical Engineering

Geometrisch bestimmtes

Konstruktieren

Dipl.-Ing. Philipp Schmiechen

Summary

Die Anforderung an eine immer höhere Wiederholgenauigkeit mechanischer Systeme verlangt nach neuen Konstruktionswegen. Diese Arbeit präsentiert als eine mögliche Methode das geometrisch bestimmte Konstruieren.

Geometrisch bestimmtes Konstruieren vereinfacht die Lösung, indem das zu konstruierende System in Starrkörper und plastisch/elastische Kontaktzonen aufgeteilt wird. Damit können die Berechnungen aufgespalten werden in globale und lokale Berechnungen.

Mit dieser Annahme vereinfacht sich die Berechnung gegenüber eines elastischen Modells erheblich, bei dem zusätzlich der interne Spannungs-/ Deformationszustand berücksichtigt werden muß.

Die Arbeit zeigt die Berechnung und wendet diese auf zwei Beispiele an: eine Werkzeughalterkupplung und ein Linearsystem.

Thesis Supervisor: Dr. Alexander H. Slocum

Title: Associate Professor of Mechanical Engineering

Acknowledgements

I would like to thank Professor Alexander Slocum for inspiring and supervising me during the research and writing of this thesis. To follow some of his many ideas was a most challenging and enjoyable experience.

The basement of Building 35, with its many research students, is witness to the perpetual battle between high-tech and low-tech. Long may it continue!

I am thankful to Haruko-san for being with me.

My love to Mom and Dad for showing the way when I only saw the wall and for making me believe when I was about to give up.

Contents

List of Figures

1. Introduction

Kinematic design is not a new design idea. It has been applied to machine design problems for centuries [1]. It is a design method that tries to respect the kinematic principle throughout the whole design process. The principle requires that the design be deterministic and statically determinate. The constraint equations will have to take only the contact forces into consideration. On the other hand, an over-constrained system is not statically determinate and does not necessarily have an easily obtainable solution to the equations of equilibrium as the internal forces and deflections need to be considered simultaneously. As many design solutions exist, the impact of external factors cannot be determined uniquely. Kinematic design tries to decouple these external factors and to associate them with their effects on the design.

Any proven design methodology tries to consider all factors of influence, but kinematic design goes one step further and makes their effects on the structure more readily computable by decoupling the factors of influence for a family of unique solutions. Through this advantage the design specifications can be met more reliably and fewer iterations will be required. Conventional design does often not allow the designer to make accurate calculations easily and depends in many cases on engineering estimates.

In this sense kinematic design is more robust than conventional design.

1.1 Background

With the demand for ever increasing accuracy, conventional design approaches its limits. It might still produce a solution within the technical specifications, but if financial aspects are considered, it becomes evident that different approaches must be employed. It is the design stage that fixes 80% of the costs of a product [2]. Therefore it is desirable to optimize the design and not only the manufacturing process. The best product will not succeed if the price does not match the desirability.

One possible alternative to many conventional design methods is the kinematic approach. To show the strength and validity of this particular approach, its design principles are reviewed and particularities are brought to attention.

1.2 Statement of Objective

This thesis shall examine the design methodology for kinematic design. Examples will be presented. The limits of the method will be described and clarified.

The thesis shall give practical guide lines for actual calculation so that designers unfamiliar with the method will be able to make calculations for their specific application.

1.3 Thesis Layout

The layout of the thesis follows closely the design process: Chapter 2 describes the ideas and theory of kinematic design and explains its advantages as compared to other design principles.

Chapters 3 and 4 are case studies that illustrate how to apply the theory to practical problems. These chapters are split into three parts: a theoretical, an idea finding, and a practical part, resulting in detailed design solutions.

Chapter 5 finally summarizes the results and Chapter 6 concludes the work with recommendations for further research.

2. Design Theory

The principle of kinematic design is well known. Although the principles of deterministic design, as it is also called, are often applied, equally often they are violated in detail or when it comes to complex problems. The same principle that applies to keep a body in a uniquely defined position holds true in detail, i.e., when a coupling interface is to be designed so that the two parts fit together in exactly the same way over and over again. Sadly, designers often rely on traditional ways to solve their problems in precision design and end up spending more effort to overcome problems inherent to the design chosen.

2.1 Comparison to Elastically Averaged Design

The most obvious example for the violation of the kinematic principle is a chair with four legs. The four legs result in an over-constrained design. Here the elastic deformation of the whole chair as a response to an applied load will keep all four legs in contact with the ground. Only in very rare, ideal cases, will the ground geometry exactly match the geometry of the chair. As assumptions have to be made on how the chair will deform, the solution will eventually be only an approximation to reality, too. This will, in most cases, reduce the predictability of the accuracy of a non-kinematic system.

With the three-legged chair all legs will be in permanent contact without the chair as a whole having to deform. Its position is unique. This statement assumes that the three legs do not lie on a line but form a triangle.

If the kinematic three-legged chair is compared to the over-constrained four-legged chair the difference is that in the former a contact of all legs will be achieved statically determinate without introducing any alignment strains into the structure while in the latter these will always be present. This puts permanent strain on the four-legged chair and can contribute to a decrease in repeatability.

On the other hand, if the chair is heavily loaded it may be desirable to distribute the load over many legs. Thus the design problem shifts to the question of how to increase the load capability of the chair. The kinematic, three-legged chair does not allow for more legs and the load capability can be improved only marginally [3], unless a compromise design is chosen.

2.1.1 Quasi-kinematic Design

If, for load reasons, a kinematic design cannot be achieved, the designer should try to keep as many advantages of the kinematic design as possible and incorporate them in a conventional design, or vice versa. The resulting design can be described as quasi-kinematic design. It can yield an effective compromise between the advantages, e.g., repeatability, of a purely kinematic design and the load capacity of an elastically averaged design.

The difference between a kinematic and a quasi-kinematic system would be in the contact zone, where the designer would rely on elastic averaging to obtain the load capacity. The number of contact regions is still kinematic but the points are allowed to become localized planes of contact. Compared to a conventional design, the elastic averaging would be spread over a minimum number of regions. Symmetry and simplicity in the contact areas will help to reduce the disadvantages

inherent the non-kinematic design. An example for a quasi-kinematic coupling design is given in Chapter 3.

2.2 Degrees of Freedom

A rigid body in space can move in the all three dimensions and can rotate about three axes, but will keep its body dimensions. Thus six variables are needed to describe the position of such a body. It is said to have six degrees of freedom, three translational and three rotational. A system of N rigid bodies has 6 N degrees of freedom. If the position of such a system is to be fixed uniquely with respect to a reference frame all these degrees of freedom must be constrained. To allow for one degree of freedom, say travel in one direction or rotation around one axis, all but one, (6 N - 1), degrees of freedom have to be constraint.

2.3 Constraining Degrees of Freedom

For static equilibrium or steady motion, the vector Equations 2.1 and 2.2 have to be solved:

$$\Sigma \boldsymbol{F}_{contact} = \boldsymbol{F}_{applied} \tag{2.1}$$

$$\Sigma \boldsymbol{r} \times \boldsymbol{F}_{contact} = \boldsymbol{M}_{applied} \tag{2.2}$$

These can be combined to

$$\begin{pmatrix} \boldsymbol{n}_1 & \cdots & \boldsymbol{n}_i \\ \boldsymbol{r}_1 \times \boldsymbol{n}_1 & \cdots & \boldsymbol{r}_i \times \boldsymbol{n}_i \end{pmatrix} \begin{pmatrix} F_1 \\ \vdots \\ F_i \end{pmatrix} = \begin{pmatrix} \boldsymbol{F}_{applied} \\ \boldsymbol{M}_{applied} \end{pmatrix} \tag{2.3}$$

where the $\boldsymbol{n}_i$ are the normal vectors of the contact forces, the $\boldsymbol{r}_i$ are the location vectors and the F_i are the magnitudes of the contact forces. Once the contact forces are known, deflections can be calculated in a straightforward manner. This contrasts the non-kinematic systems where forces and deflections must be determined simultaneously which can result in very complex calculations. As a result, too many systems are built whose designs were never properly analyzed.

2.3.1 Existence of a Solution

If, in Equation 2.3, $i = 6$ then the matrix is square. The set of equations has exactly one solution for the six unknown magnitudes of the contact forces F_i if the determinant of the matrix is non-zero. Mathematically the problem is well posed if the determinant is not close to zero. The same can be expressed in terms of a condition number [4], which is defined as the ratio of the largest eigenvalue to the smallest eigenvalue of the matrix. The problem is ill-conditioned if the value of this parameter is large, so that its reciprocal approaches the machine precision. For a singular matrix it would be infinity. With increasing value the numerical solution of the problem becomes polluted by round off errors introduced by the limited number presentation. Thus, the value of the condition number provides for a valuable check for the quality of the design.

For example, in the case of the three-legged chair, which was assumed to be kinematic, the problem is not well posed if all three legs lie on one line.

In mechanical terms a large condition number will indicate that two or more contact forces are almost parallel. A good design will avoid this situation in the first place and Equation 2.3 can be assumed to be well posed.

For an over-constrained, non-deterministic design on the other hand $i > 6$. In this case, a solution to Equation 2.3 can only be given in a least square sense as more unknowns than equations exist. Furthermore, and more troublesome, the whole elastic deformation state has to be taken into account to satisfy the constraint equations and a more complex solution, often involving finite elements, must be sought if one wants to be able to accurately predict the dimensional performance of the design.

2.4 The Deterministic Dilemma

The deterministic arrangement faces the following problem: the design may be deterministic but the material is not. It needs little explanation as to how far this affects the computation of the kinematic design: The static solution of the above equations assumes that the directions of all acting forces are known. This in turn excludes two phenomena that are omnipresent: friction and finite contact areas. Friction will affect the stability and the admissible yield stress will limit the load capacity.

The deterministic design, to give a good approximation, has to consider these factors by calculating and minimizing their effects on the design.

2.5 Stability

Stability can be affected by friction. In a poor design the frictional force might prevent the kinematic system from reaching its uniquely defined force distribution and thus its location as assumed in the solution of Equations 2.1 and 2.2. If the preload is insufficient to overcome the acting friction force, the design will not exhibit a distinct equilibrium position where the potential energy is minimized, but will have only an indifferent minimum with a number of possible positions. During operation this will reduce the repeatability and will degrade the overall performance of the design. On a micro level, friction seems to be affected by the surface finish [5]. Experiments indicate that the repeatability is a function of the surface roughness.

Maxwell in [6], referencing Ball [7], gives a geometrical interpretation of stability:

> "When an instrument is intended to stand in a definite position on a fixed base it must have six bearings, so arranged that if one of the bearings were removed the direction in which the corresponding point would be left free to move by the other bearings must be as nearly as possible normal to the tangent plane at the bearing.
>
> "(This condition implies that, of the normals to the tangent planes at the bearings, no two coincide; no three are in one plane, and either meet in a point or are parallel; no four are in one plane, or meet in a point, or are parallel, or, more generally, belong to the same system of generators of an

hyperboloid of one sheet. The conditions for five normals and for six are more complicated.)[6]"

This quite intriguing explanation of stability in geometrical terms is not easily evaluated and designers might be inclined to follow only the simple rules up to three and four forces, if not intuition replaces the proper analysis completely.

If the stability analysis is put in mathematical terms, it reduces to a simple condition on the invertability of the matrix in Equation 2.3. Thus stability is closely related to the condition number that was introduced in Section 2.3.1. Its magnitude was then associated with the quality of the design.

As said above, the condition number will be large if the matrix is close to singular and will be infinite for a singular matrix. Both cases hinder the inversion of the matrix. Even though near-singular matrices are invertible in theory, round off errors will give random results.

In mechanical terms a singular matrix means that the forces are linearly dependent, and the same effect or force state could have been achieved with fewer forces. This implies that the six degrees of freedom are not adequately constrained in this configuration.

2.6 Load Capacity

For the kinematic design, point contact between the bodies is desired. For true contact points any applied load will yield infinite surface stresses. In reality these will instantaneously cause deformations and will extend the point generally to an elliptical contact area. This effectively limits the stress to the yield stress. The

allowable contact stresses are the most severe limitations on the kinematic design. Typically, the allowable stress should only be a fraction of the maximum material stress in order to maintain elastic behavior and dimensional stability.

2.6.1 Hertz Contact Theory

Hertz [8] originally developed the theory for contact stresses in elastic materials. In his derivation he assumed the existence of an elastic regime and that the dimensions in the contact area itself are much smaller than those of the touching bodies. Starting point of Hertz' derivation are the equations of Boussinesq that describe the deflections and stresses in a semi-infinite body acted upon by a point force.

Most textbooks [3, 9, 10] follow Hertz in reducing the general case of two arbitrarily shaped bodies to the case of a sphere touching a plane. The reason for doing so is that for this case the exact analytical solution exists and is known. This reduction requires two steps: the shape of the bodies near the small contact area must be approximated to ellipsoids and the general case for two ellipsoidal bodies must be transformed into the case of a plane touching a sphere by introducing equivalent material properties and dimensions.

Figure 2.1 illustrates the geometry of the interface in the general case of two arbitrarily shaped bodies with radii R_{major1}, R_{minor1} and R_{major2}, R_{minor2}.

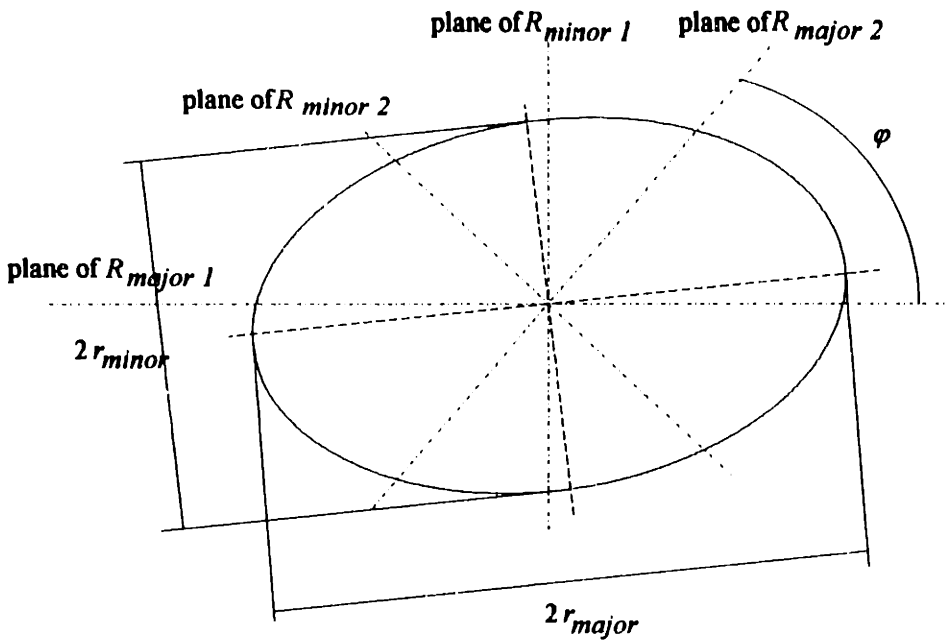

Figure 2.1: Geometry of the contact zone for bodies of arbitrary shape in the contact zone.

The 'equivalent' radius R_e of the sphere and the 'equivalent' modulus of elasticity E_e are calculated from Equations 2.4 and 2.5, respectively:

$$\frac{1}{R_e} = \frac{1}{R_{major1}} + \frac{1}{R_{minor1}} + \frac{1}{R_{major2}} + \frac{1}{R_{minor2}} \tag{2.4}$$

$$\frac{1}{E_e} = \frac{1-\nu_1^2}{E_1} + \frac{1-\nu_2^2}{E_2} \tag{2.5}$$

with ν the Poison ratio for the material. For concave bodies the radii are to be taken negative and a plane has infinite curvature. With these values the radius of an 'equivalent' circular contact area can be computed:

$$r_{contact} = \left(\frac{3FR_e}{2E_e}\right)^{1/3} \tag{2.6}$$

In the general case the contact area will be elliptical. To obtain its semi-axes r_{minor} and r_{major}, scaling factors α and β have to be calculated. The general computation requires the solution of elliptical integrals. Most textbooks, e.g., [9], give tables for the scaling factors, [3] gives a polynomial approximation. Compared to the exact solution that requires the computation of an elliptical integral, this reduces the computational effort and makes it amenable to computation. The auxiliary quantity $\cos(\vartheta)$ can be calculated from Equation 2.7:

$$\cos(\vartheta) = \left\{\left(\frac{R_e}{R_{minor1}} - \frac{R_e}{R_{major1}}\right)^2 + \left(\frac{R_e}{R_{minor2}} - \frac{R_e}{R_{major2}}\right)^2 + 2\left(\frac{R_e}{R_{minor1}} - \frac{R_e}{R_{major1}}\right)\left(\frac{R_e}{R_{minor2}} - \frac{R_e}{R_{major2}}\right)\cos 2\varphi\right\}^{1/2} \tag{2.7}$$

This quantity serves as an index to Table 2.8 or as a variable for the interpolation for the calculation of the scaling factors α and β, depending on the method of computation.

$\cos(\vartheta)$	α	β	λ
0.00	1.000	1.000	0.750
0.10	1.070	0.936	0.748
0.20	1.150	0.878	0.743
0.30	1.242	0.822	0.734
0.40	1.351	0.769	0.721
0.50	1.486	0.717	0.703
0.60	1.661	0.664	0.678
0.70	1.905	0.608	0.644
0.75	2.072	0.578	0.622
0.80	2.292	0.544	0.594
0.85	2.600	0.507	0.559
0.90	3.093	0.461	0.510
0.92	3.396	0.438	0.484
0.94	3.824	0.412	0.452
0.96	4.508	0.378	0.410
0.98	5.937	0.328	0.345
0.99	7.774	0.287	0.288

(2.8)

The semi-axes of the elliptical contact zone are:

$$r_{minor} = \alpha \cdot r_{contact} \tag{2.9}$$

$$r_{major} = \beta \cdot r_{contact} \tag{2.10}$$

Once the interface geometry is determined, the deflection and the stress state in the two bodies can be obtained.

The contact pressure can be calculated from Equation 2.11:

$$\sigma_{contact} = \frac{3/2\,F}{\pi\, r_{major}\, r_{minor}} = \frac{1}{\pi\alpha\beta}\left(\frac{3FE_e^2}{2R_e^2}\right)^{1/3} \tag{2.11}$$

While this maximum compressive stress occurs directly at the interface, the maximum shear stress occurs underneath the surface:

$$\tau_{contact} = \sigma_{contact}\left(\frac{1-2\eta}{4} + \frac{1}{9}\sqrt{2(1+\eta)^3}\right) \tag{2.12}$$

These two values can be used in the failure hypotheses according to the material: for materials exhibiting an elastic/plastic behavior like metals, a maximum normal stress hypothesis will be employed, for brittle materials like ceramics a maximum shear stress hypothesis will be used.

A safety factor will be used to accommodate for uncertainties in the calculation and the loading. This is to ensure that the plastic regime is not reached. As described in [3], the stress ratio should be kept small, as a high ratio might degrade the long-term performance of the coupling depending on the wear behavior of the interface material.

The change in distance between two points in the two bodies far away from the interface is given by:

$$\delta = \lambda\left(\frac{2F^2}{3R_eE_e^2}\right)^{1/3} \tag{2.13}$$

where λ is taken from Table 2.8. This quantity and the two radii of the elliptical contact area, Equations 2.9 and 2.10, have to be small compared to the dimensions of the bodies to satisfy the assumptions made in the derivation of the theory.

2.6.2 Discussion

For an economical and high performance design of a kinematic system, both the Hertzian contact stresses, (2.11) and (2.12), and the contact deflection, (2.13), should be small. If the contact normal forces are given, Equations 2.1 and 2.2, this implies that the product $\alpha\beta$ should be maximized. Table 2.8 indicates that this is the case for $\cos(\vartheta) = 0$. The radius of the equivalent sphere, (2.4), and the equivalent modulus of elasticity, (2.5), occur in the calculation of both stresses and deflection and thus must be optimized with respect to both quantities. The equivalent radius for small values in both cases needs to be large but the equivalent modulus of elasticity needs to be small for the stresses through a larger contact area and large for a small deflection.

For high precision components where one cannot sacrifice accuracy or repeatability, this optimization problem will be restated: For a given contact force and a required maximum deflection, find the minimum size and geometry of the design as expressed in the equivalent radius.

A short note is in place here on how to interpolate values from Table 2.8: One possible way is to choose a higher order polynomial, as was done in [3], where two fifth order polynomials are being used. If the data are sketched as a function of ϑ instead of $\cos(\vartheta)$, as e.g. in [9], then it can be anticipated that a lower order approximation should be sufficient to cover the whole interval accurately. This is

due to the much smaller gradient for the functional relationship in ϑ. Employing a non-linear root finder, e.g. the FMINS function in MATLAB™ [11] or one of the many in [4], the following approximations for α, β and λ can be computed:

$$\alpha \approx 1.939e^{-5.26\vartheta} + 1.78e^{-1.09\vartheta} + 0.723/\vartheta + 0.221 \tag{2.14}$$

$$\beta \approx 35.228e^{-0.98\vartheta} - 32.424e^{-1.05\vartheta} + 1.486\vartheta - 2.628 \tag{2.15}$$

$$\lambda \approx -0.214e^{-4.95\vartheta} - 0.179\vartheta^2 + 0.555\vartheta + 0.319 \tag{2.16}$$

These values are accurate to less than 0.5% to the tabulated values in Table 2.8. Even though the change is subtle, it will help to simplify the implementation.

2.7 Error Motions

The deflections of all contact points as calculated in Equation 2.13 will determine the final position of the two coupling members with respect to each other. This motion is in principle undesired and can be considered an error motion.

The distances of the contact points from each other are assumed to be fixed. Due to the deflections, the contact points will move to maintain their distances. This motion depends on the geometry and the applied loads but is, in the absence of friction, a deterministic problem [12]. The deflections as calculated from Equation 2.13 and the compensating motions just described give the new coordinates of the contact points relative to the original positions δ_i, $i = x,y,z$.

From the differential linear motions the angular motions ε_i, $i = x,y,z$ can be determined.

The full description of the location of the two parts with respect to each other requires six quantities: three translational error motions δ_i and three rotational error motions ε_i. These are conveniently arranged in a transformation matrix. If the coordinate system is located in the point for which the transformation matrix was calculated, the error motion of an arbitrary point relative to the origin can be calculated from Equation 2.17:

$$\boldsymbol{r}^{error} = \begin{pmatrix} 1 & -\varepsilon_z & \varepsilon_y \\ \varepsilon_z & 1 & -\varepsilon_x \\ -\varepsilon_y & \varepsilon_x & 1 \end{pmatrix} \boldsymbol{r}^{ideal} + \begin{pmatrix} \delta_x \\ \delta_y \\ \delta_z \end{pmatrix} \tag{2.17}$$

or,

$$\boldsymbol{r}^{error} = \mathbf{T}\boldsymbol{r}^{ideal} + \boldsymbol{\delta} \tag{2.18}$$

For zero error motions $\boldsymbol{r}^{error}$ and $\boldsymbol{r}^{ideal}$ coincide. The most convenient way to proceed from Equation 2.13 is to obtain the transformation matrix-deflection pair $(\boldsymbol{T}, \boldsymbol{\delta})$ for any one of the contact points and then use Equation 2.18 to obtain the transformation matrix-deflection pair for the coupling center as the origin of the body fixed coordinate system [12]. This procedure avoids the unnecessary introduction of further assumptions about the combination of the translational and the rotational error motions of the contact points to the total error motions of the coupling [3].

The compliance of the design in all six degrees of freedom is given by the ratio of the error motions and the applied forces and moments, respectively.

For a preload has a high repeatability in both magnitude and direction, the deflections resulting from the preload are known and can be compensated for. Thus only the motion due to the applied loads must be considered as an error motion.

With Equation 2.17 the principle of the amplification of angular error motions can be explained easily: Abbé's principle, [13], states that the angular error motions are amplified by the projected distance of the point in consideration to give additional translational error motion. Thus small angular error motions can have a large impact on the total error motion of the system. Translational error motions are carried over without amplification

2.7.1 Center of stiffness

A result of Abbé's principle is that there exists one point in the system for which the angular error motions are zero if a load is applied. This point is called the center of stiffness. If forces are applied at this point, the system will only react by translational motion. To underline the importance of the center of stiffness the coordinate system of the coupling should originate at this point.

If the k_i are the vectorial stiffnesses acting at locations r_i then the center of stiffness is located at:

$$r_{CS} = \frac{\Sigma k_i r_i}{\Sigma k_i} \tag{2.19}$$

2.8 Conclusions

It seems to be favorable to design with only the kinematic paradigm if high repeatability is required but one must be careful to make the joints strong enough to prevent contact stress problems. Quasi-kinematic design can be used to increase the load capacity without perishing too great a reduction in repeatability. Even in a kinematic design, reality imposes a limit on the achievable stiffness and so some elastic averaging will occur on the footprint level. Hertz' theory can be used to predict the magnitude of the contact stresses and serves as an indicator of the suitability of the design for a given task.

3. Case Study 1: Kinematic Coupling Design

The goal of this case study was to show the application of kinematic design to a component in an existing machine, to gage its performance and thus to prove the validity of the calculations and the underlying theory [15]. A good example to consider is a tool holder coupling during machining. This a zero degree of freedom system. For the replacement of the existing tool holder it was sought to achieve a level of repeatability of better than 1 μm in the sensitive directions. Sensitive directions are directions in which accuracy or repeatability are required. An example is a lathe, where the radial location of a tool is typically more important than the tangential direction. A further constraint was to maintain the physical dimensions and interfaces to ease the transition to the new design.

For lightly loaded systems, kinematic couplings have been shown to give increased repeatability at lower cost compared to a conventional design based on elastic averaging [3, 14], shown in Figure 3.1.

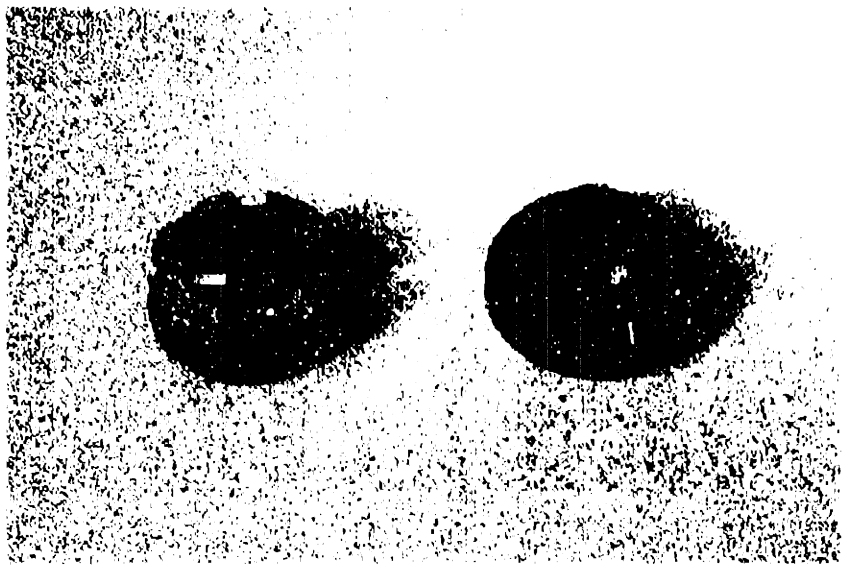

Figure 3.1: Conventional tool holder coupling.

In modern machining operations repeatability gains more and more importance as it is the key property in today's CNC manufacturing environment. Designers of CNC machines solved most problems associated with resolution and accuracy as defined in [16].

A good example for the importance of repeatability is the machining / measurement / correction process on a CNC machine and a coordinate measurement machine (CMM). After CNC machining the work-piece has to be measured at the CMM. From the errors, the necessary corrections are calculated. This process assumes that the part can be placed in the same position in which it was held during the initial machining. Only then the corrections will be made at the proper place and thus will yield an increase in the overall accuracy of the work-piece.

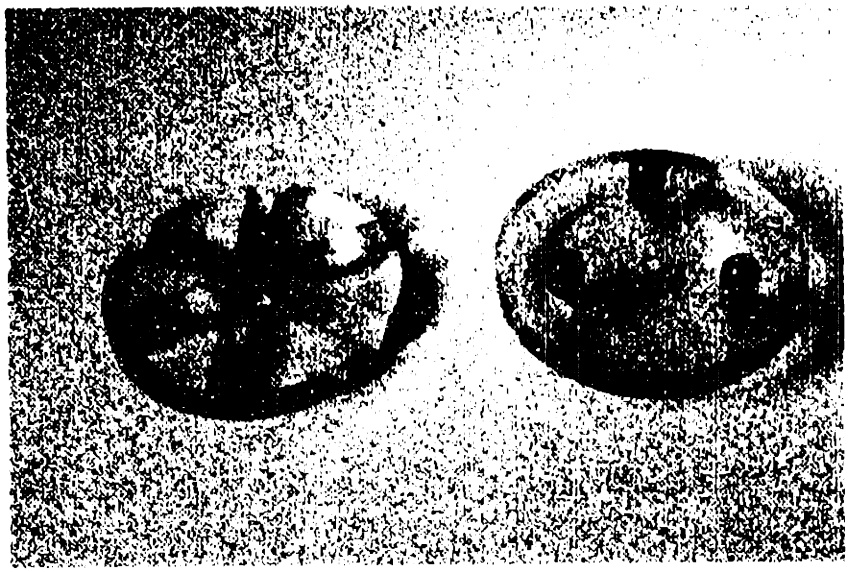

Figure 3.2: Kinematic three groove coupling.

A kinematic design, as shown in Figure 3.2, is a design that employs the minimum number of contact points to constrain the position of rigid bodies with respect to each other. If in three dimensions no relative motion between two parts is allowed then six contact points will be required for the six degrees of freedom, three translational and three rotational. Once these points are defined the position of the coupling is uniquely defined.

The repeatability of the kinematic coupling is restricted by the elastic properties of the material at the contact points. The problem reduces to the maximum allowable Hertzian stress for the material. This is the limiting factor of the kinematic design. As the forces are transmitted through 'points', the contact stresses rise quickly and can easily reach the plastic regime, if it exists. If plastic deformation occurs the relation of the two coupling members has changed permanently, the coupling lost its repeatability.

3.1 Problem Definition

It is necessary to improve the repeatability of an existing coupling for a tool holder for a precision machine tool to less than 1 μm. It is anticipated that this will economically only be possible by applying kinematic design principles.

To easily evaluate the new design it is desirable to maintain the interface dimension.

3.2 Specifications

The repeatability in the sensitive directions X and Y, as shown in Figure 3.3, shall be better than 1 μm in a finishing cut, here assumed to be a 3D force vector (X = 10 N, Y = 10 N, Z = 20 N) acting at a distance of 50 mm from the coupling center. For a rough cut with an estimated force (X = 20 N, Y = 20 N, Z = 100 N) it should be below 5 μm.

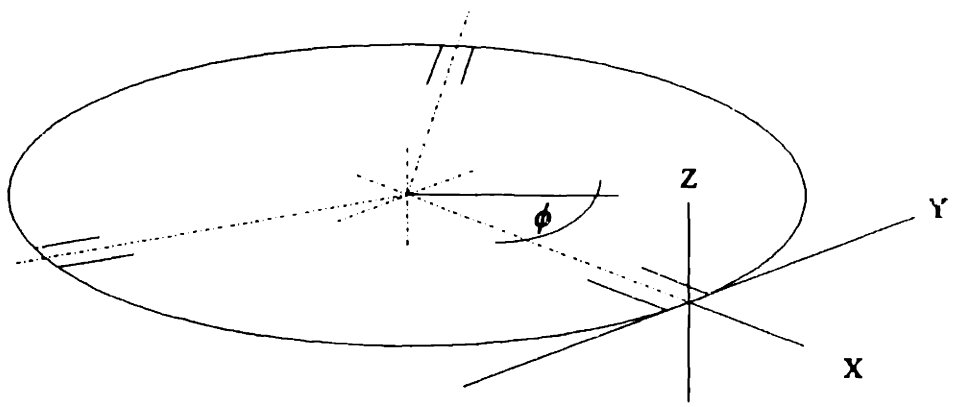

Figure 3.3: Coordinate System. The sensitive directions are X and Y.

3.3 Solution

The quality of an elastic averaging coupling depends very much on the quality of the manufacturing process. Furthermore the coupling needs a wear-in period in which existing surface irregularities will be smoothened. In contrast to that, the kinematic design allows for larger manufacturing tolerances and needs essentially no wear-in time. It delivers high repeatability on the order of the surface finish of the component right from the beginning. Thus a kinematic design will lower the cost while increasing the repeatability.

The calculations are based on a spreadsheet developed by Slocum [3], given in Appendix A. This spreadsheet provided the computational base for calculating the homogeneous transformation matrix (HTM) for the error of the coupling in a fixed coordinate frame. Multiplying by the vector to the point where the error motions are to be reported the deflection at this point is obtained.

Inputs to the program are the geometry of the coupling and the preload and applied load acting upon the coupling. The output is the maximum stress and the deflection at the point of interest.

In order to perform a sensitivity analysis changes to the program were necessary to allow the applied force vector to be placed arbitrarily. The investigation was limited to a 3 balls in 3 groves, 120° configuration coupling.

Available parameters involved in the design of the coupling are the geometry, the interface material, the surface finish and the manufacturing process. The geometry is set by design constraints and the necessary load capability. The properties of the material at the interface will determine the allowable stresses and the Hertzian stresses therefore limiting the load capability of a coupling of any

given geometry. This does not only cover the immediate interface area but the coupling as a whole as assumptions are made that the coupling acts like a rigid body or will at least not bend considerably under the applied loads. The surface finish will influence the repeatability and the long term behavior of the coupling. The larger the surface roughness the smaller will be the initial repeatability [16]. The spreadsheet assumes that we are dealing with half spheres. How close the design approaches this idealization depends very much on the way the balls are attached to the supporting structure.

3.3.1 Interface Manufacturing

The attachment of the balls is important to the performance of the coupling. Ideally the balls would be an integral part of one of the coupling members. If they are not, the attachment will act like another interface. It will introduce error motions in the same way as the coupling does. The total error motion matrix for the two coupling members would then be a superposition of the coupling error matrix and the ball interface error matrices. This total error matrix enters the error budget of the system or machine and, as it was the primary goal to minimize the error motions and increase the accuracy, the ball interface must be designed so that its error motions are much smaller than those of the coupling

The ideal way for the balls to be manufactured and attached to the coupling member is to machine them into the part, either by milling, grinding or electro discharge machining to name some, followed by polishing. This can be quite costly as the requirement of the surface finish are those of the repeatability. However, polishing of spherical surfaces is a well known process. For cast parts this can be

an economical way to manufacture the coupling. Especially for consumer products, balls and grooves can be integral parts of injection moulded plastic parts. In this manner, extremely high repeatability can be obtained for very little cost and minimal reliance on skilled labor.

Another way is to take standard parts with a high surface finish and attach them to the coupling member. The balls could be press fit into cylindrical holes as shown schematically in Figure 3.4, where the ventilation hole avoids excessive pressure build up when the ball is pressed in.

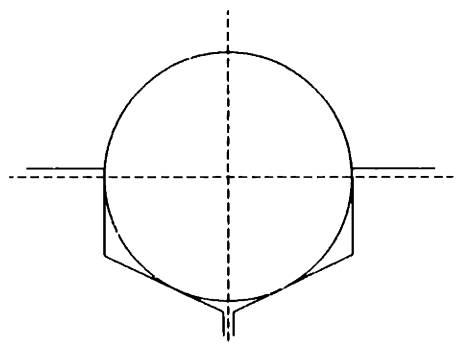

Figure 3.4: Ball attachment through press fit.

Depending on the materials used, balls and holes would deform elastically and plastically. Only the elastic deformation contributes to the desired interface stiffness while any plastic deformation introduces inaccuracies that were not accounted for in the calculation. The optimal press fit would just reach the yield stress locally so to guarantee maximum stiffness. Where only elastic material behavior is present, e.g. when the balls and/or the coupling member is made from

ceramics, care has to be taken not to damage the parts permanently. Possible procedures would include to thermally expand the hole, again a procedure not without problems.

Where the manufacturing cannot be controlled accurately enough or where it would be to costly to do so, a less desirable solution would be to epoxy-glue the balls into tight fit holes. Here it is even more important to obtain contact between balls and holes, Slocum [3] proposes to press balls into the seats prior to the final assembly so as to cause effects akin to brinelling, [5, 17]. This reduces unwanted surface elevations or positive skewness and increases the actual available contact points. This potentially increases the long-term accuracy and repeatability.

The discussion above covers the manufacturing of the grooves equally, i.e., the grooves could be made from standard cylinders, e.g., dowel pins, pressed into slots according to Figure 3.5.

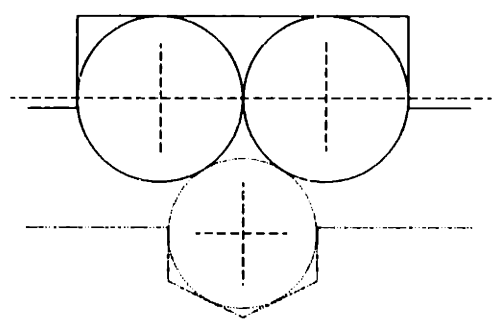

Figure 3.5: Two cylinders forming a groove.

However, the contact stresses would be high and the stiffness would be low compared to a Gothic arch ground into the surfaces. All the problems mentioned

above apply. They are even more complicated because the two cylinders contact each other. The manufacturing of both the slots and the cylinders has to be controlled much more accurately as imperfections would force the cylinders out of the slots.

Which part actually carries the balls and which one the grooves cannot be answered in general but will be determined by factors such as cost or requirements resulting from the specifications. The number of expensive operations should be minimized. If there is one stationary part and more than one moving part, then the more expensive fixturing would go typically into the stationary part. For example, if the grooves are ground into the part, the ball fixturing might be the more expensive operation and thus would be manufactured into the stationary part.

In the presence of dust particles, the grooves should point in the same direction as gravity. Beside of that, great care should be taken to keep the interface clean. For couplings being partly manufactured from steel, this demands for lubrication. This layer of lubrication will not contribute to the load capability but will help to ensure a rust-free contact area. This might be necessary for stainless steel parts, too. Lubrication can also help to overcome friction and thus ensure repeatability.

As can be seen from this discussion, the attachment of the balls in the holes relies heavily on the principle of elastic averaging. what is an inferior principle for the coupling as a whole can be the only feasible mechanism in detail!

3.4 Theory

The contact stresses in the coupling interface will have to be checked as they will limit the load capability of the coupling most severely. Starting from the general

theory outlined in Chapter 2, most of the equations can be simplified. Figure 3.6 shows the geometry of the coupling interface:

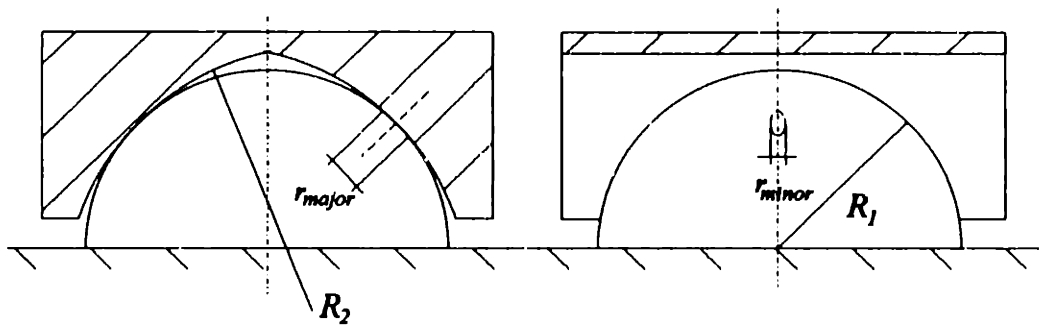

Figure 3.6: Geometry of the contact zone for a ball touching a Gothic arch.

For the equations it is important to note that the radii for the sphere are the same, $R_{major1} = R_{minor1} = R_1$, and that therefore there is no distinct direction , or $\varphi = 0$. For the groove, $R_{minor2} = R_2$ and $R_{major2} = \infty$. Notice that the groove radius is to be taken negative in the equations as it describes a concave shape. Equations 2.4 and 2.7 reduce to:

$$\frac{1}{R_e} = \frac{2}{R_1} + \frac{1}{R_2} \tag{3.1}$$

$$\cos(\vartheta) = \left|\frac{R_e}{R_2}\right| = \left|\frac{R_1}{R_1 + 2R_2}\right| \tag{3.2}$$

The load capability varies with $\cos(\vartheta)$, [9]. A compromise design for small deflections and small contact stresses yields $|R_2/R_1| \approx 1.2$, [3]. The spreadsheet in Appendix A follows this description closely but employs a different method to obtain the error motions.

If the load capability was to be increased, a quasi-kinematic design could be employed. In this case one can think of it as follows: Cylinders lie in straight grooves, at the contact lines they are leveled off so that they have rectangular contact areas. This last step is the departure of the design from a purely kinematic design. The thought experiment can be concluded by replacing the cylinders by planes machined directly into both parts. The symmetry in this design extends over the two parts, they are in fact identical at the interface [18].

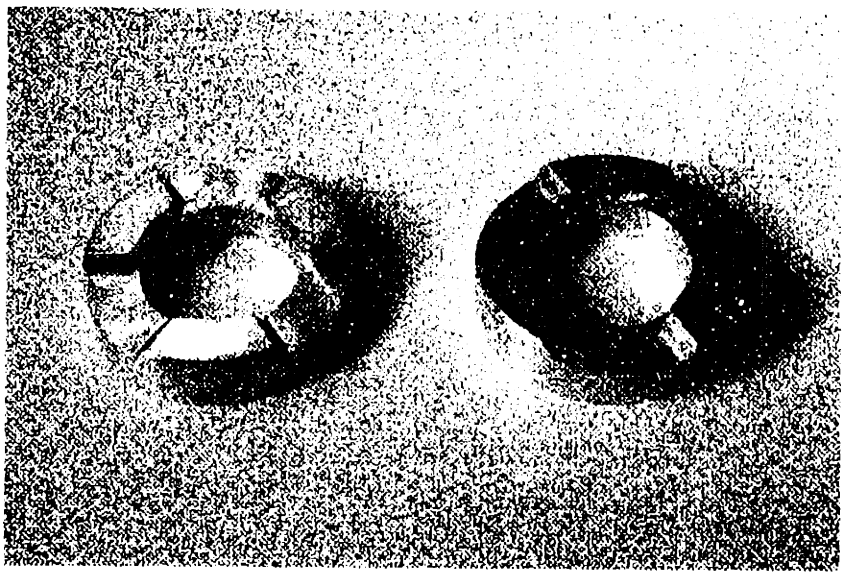

Figure 3.7: Quasi-kinematic Coupling.

3.5 Results

The performance of a tool holder coupling as predicted by the theory are summarized in Figures 3.8 through 3.11 for a standard coupling made from hardened 62 HRC steel. The deflections vary sinusoidally with the angle. After 120°, the starting position is reached again as expected for symmetry. The X and Y deflection are offset by 90° to each other, equal to a 30° angle in Figure 3.8 as there is a 120° symmetry. Figure 3.8 shows the deflections in the X, Y and Z directions in the rotating coordinate frame, normalized with respect to their value at 0°. The coupling had a 44 mm diameter with 8 mm balls so as to be closest to the existing design envelope in use by an industrial partner. The radius of the groves was chosen to be 4.8 mm and the groves contact the balls under 45°. This will give a balanced stiffness in the X and Y directions. The preload in this example was 500 N, the force of a finish cut was applied at a distance of 52 mm from the geometric center of the coupling.

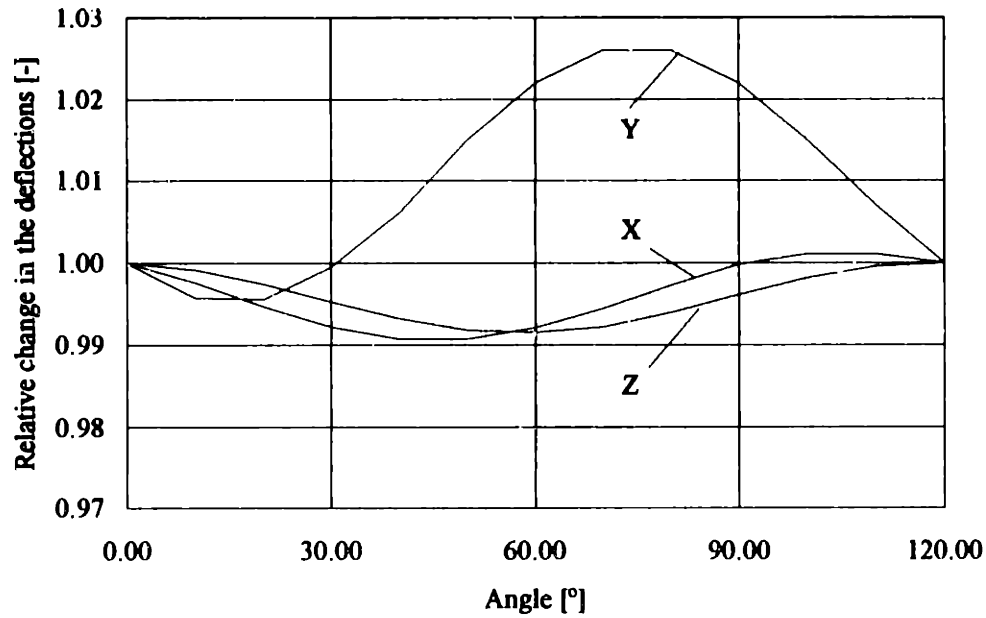

Figure 3.8: Variation of the error motions in X, Y, Z direction with the angle.

The Y direction shows the largest variation with still only 2.5%. In absolute terms the Z deflection is largest with 0.8 μm but as said before, Z is not a sensitive direction. The largest deflection in one of the sensitive directions is the one in the X direction with about 0.25 μm, which is well below the 1 μm set forth in the specifications. This proves the feasibility of the kinematic coupling in this application. It has been achieved while maintaining as much compatibility with the existing design as possible. Only the immediate coupling interface will have to be changed.

To show the robustness of the new coupling with respect to changes to design parameters, the change of the deflection in the X direction as the largest deflection in a sensitive deflection was checked.

Going back to Equation 2.13 it was expected to see a variation proportional to $R_e^{-1/3}$ and $F^{2/3}$. The size of the coupling enters only indirectly through the moment lever of the contact forces, Equation 2.2, and affects the deflection inversely proportional. Figure 3.9 shows the change for varying coupling diameter, Figure 3.10 for varying ball diameter and Figure 3.11 that for varying preload.

The coupling diameter was varied in the neighborhood of the diameter of the existing coupling. Figure 3.9 shows the essentially inversely linear relation between deflection and coupling diameter.

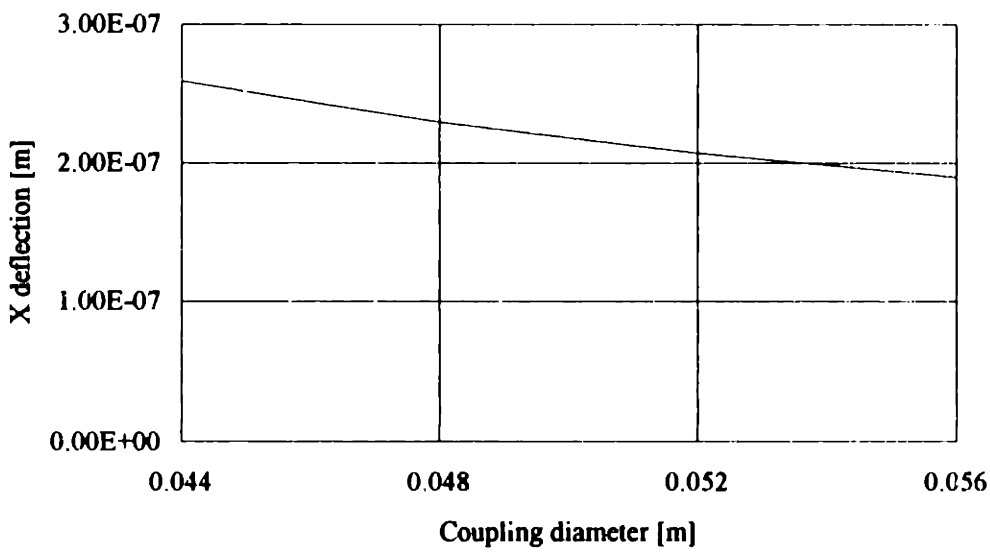

Figure 3.9: Variation of the X error motion with the coupling diameter.

As predicted by Equation 2.13, the change in ball diameter is not linearly related to the deflection, but for the small range of interest a linear relation can serve as first order approximation.

Figure 3.10 suggests that the designer has the choice to smaller balls if space is at a premium.

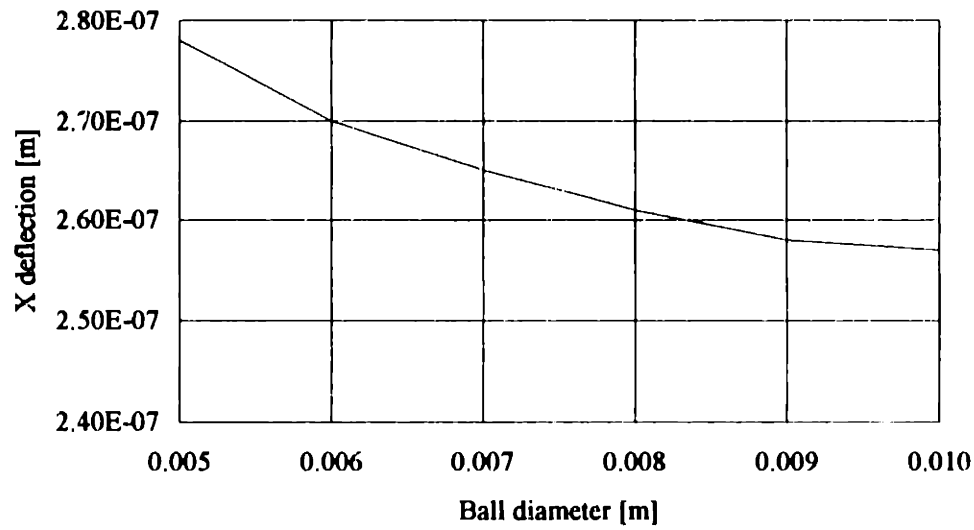

Figure 3.10: Variation of the X error motion with the ball diameter.

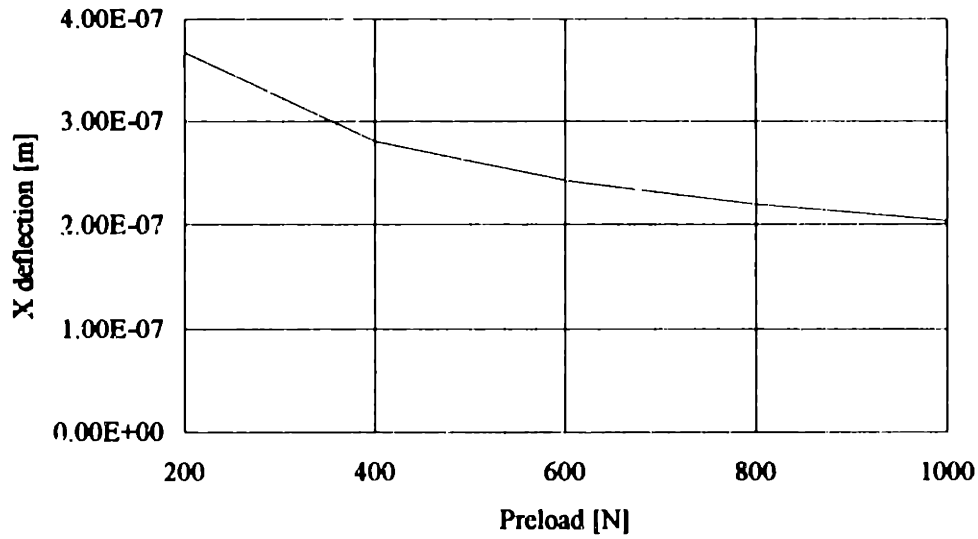

Figure 3.11: Variation of the X error motion with the preload.

Figure 3.11 shows the sensitivity of the deflection to changes in the preload. Within large limits the deflection varies almost linearly with the preload, as expected from Equation 2.13. From 400 to 1000 N 10% increase in the preload gives only 2% decrease in the deflection.

From the decrease of the error with increasing preload must not be concluded that the preload should be governed by the allowable stress only, but as mentioned in Section 2.7, the repeatability of the preload has to be taken into account. Figure 3.12 shows the effects of errors in the preload magnitude on the deflections in the Z direction. As expected, the error motion varies linearly with the relative preload error.

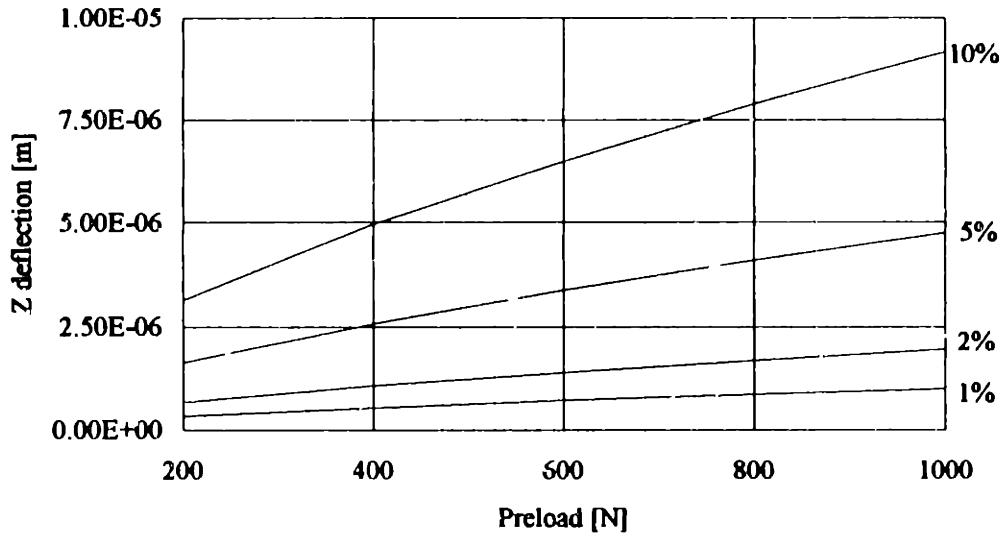

Figure 3.12: Effect of preload error on the repeatability.

This indicates that the preload should be kept as low as possible, compromising the advantages in Figure 3.11 and the disadvantages in Figure 3.12.

Varying the applied load showed the largest effect. The two operations estimated were a rough cut with a force vector (X = 20 N, Y = 20 N, Z = 100 N) and a finish cut with (X = 10 N, Y = 10 N, Z = 20 N). The resulting deflections were (X = 0.59 μm, Y = 0.17 μm, Z = 4.5 μm) and (X = 0.26 μm, Y = 0.09 μm, Z: 0.85 μm) respectively. All deflections varied almost linearly with the respective force component: X, Y doubled, Z increased about 5 times. For the rough cut the deflection in Z exceeds 1 μm but during a finish cut even this deflection in the insensitive direction stays below far 1 μm. The deflections in the sensitive directions stay always below 1 μm.

The mechanical drawings for the coupling are shown in Appendix B. In the coupling as drawn, ceramic balls will be used because of their higher load capability. The coupling is compact and it was possible to maintain the interface dimensions. Test will hopefully be conducted by next summer.

3.6 Conclusions

Under the assumptions made it seems to be possible to replace the existing coupling by a coupling design using the principle of kinematic design. Uncertainties are inherent to the estimation of the force vector and some of the dimensions. The latter is of less importance than the former as the performance of the coupling seems to be relatively robust with respect to changes in the geometry. The estimation of the force vector would have to include the dynamics as this will largely govern the maximum of the applied load.

For a kinematic coupling, the design of the groove and the attachment of the balls are as important as the cleanliness of the coupling during operation. The error motions of the ball attachments will directly affect those of the coupling. The long-term repeatability is of the order of the surface finish, and thus dirt particles can reduce the performance of the coupling. However, point contact means that there is a greater chance that the dirt will be pushed aside. In an elasitcally averaged system, dirt is more easily entrapped.

4. Case Study 2: Linear Motion Carriage Design

To illustrate the application of kinematic design for a one degree of freedom system, a linear motion system was redesigned to replace a recirculating ball-type linear bearing. The design of the kinematic system follows closely a design by Slocum for an industrial client. Many details are noteworthy and this chapter will concentrate on these details and the testing of the design. Recommendations for its simplification are developed.

4.1 Problem Definition

A precision linear motion device was to be designed with the following specifications: 500 mm of travel, 15 μm overall straightness, less than 0.4 μm straightness error with wavelengths 0.5 mm to 10 mm, velocity control accurate to 0.5%, load capacity of 10 kg, and a production cost for 2000-3000 units per year of less than $2000.

4.1.1 Conventional Design

The conventional way to solve the problem for the intended application in a printer would be to use a linear motion guide, i.e. a profile rail with circular arch grooves and bearing blocks with recirculating balls, and driven by a leadscrew. The carriage is attached to four bearing blocks that ride on the rail as illustrated in Figures 4.1 and 4.2.

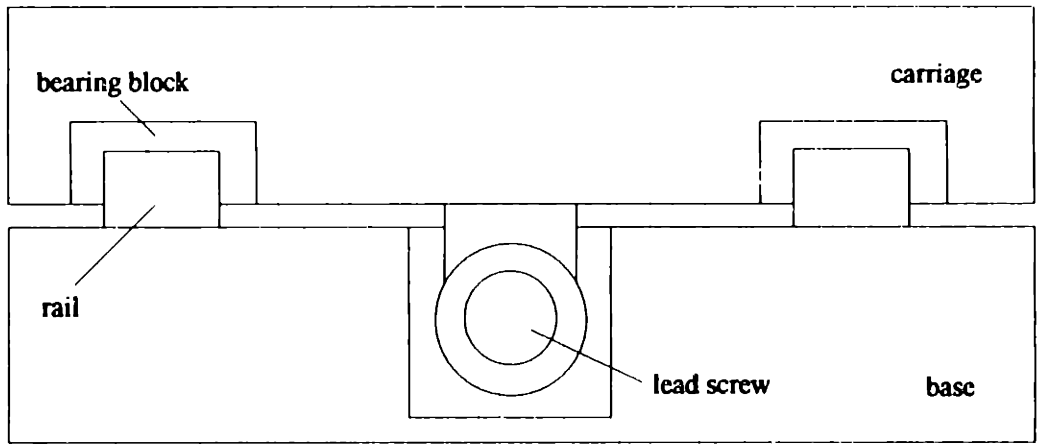

Figure 4.1: Conventional carriage design after [3].

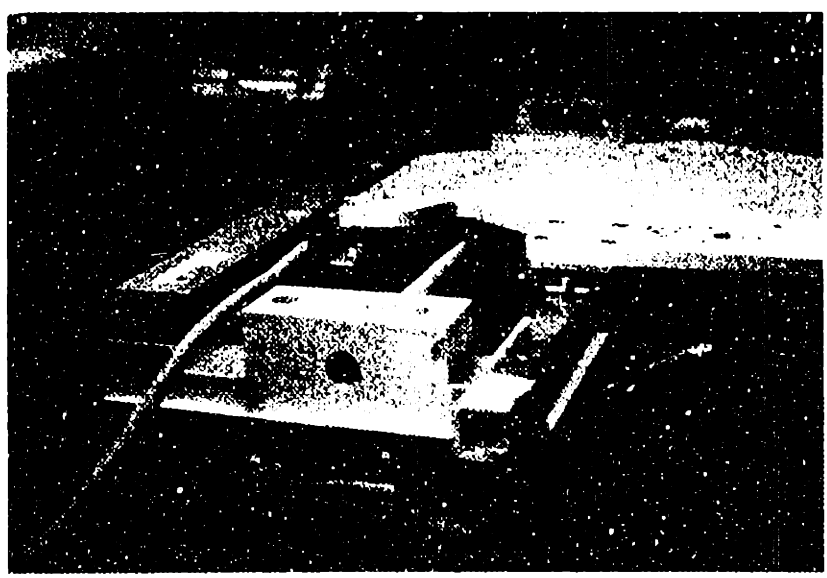

Figure 4.2: Client's conventional solution for a linear motion system.

An issue associated with this conventional design is the alignment of the two rails and the leadscrew. As the system is over-constrained, great effort has to be made during assembly to ensure accuracy and life. Furthermore the cost of skilled labor is becoming more prohibitive and a more robust design with respect to ease of assembled accuracy is clearly desirable.

A potentially better design in terms of accuracy and cost was developed using the kinematic design paradigm. The carriage is supported by five precision bearings in a vee and a flat arrangement on a single rail and preloaded by a friction drive roller, as depicted in Figures 4.3 and 4.4.

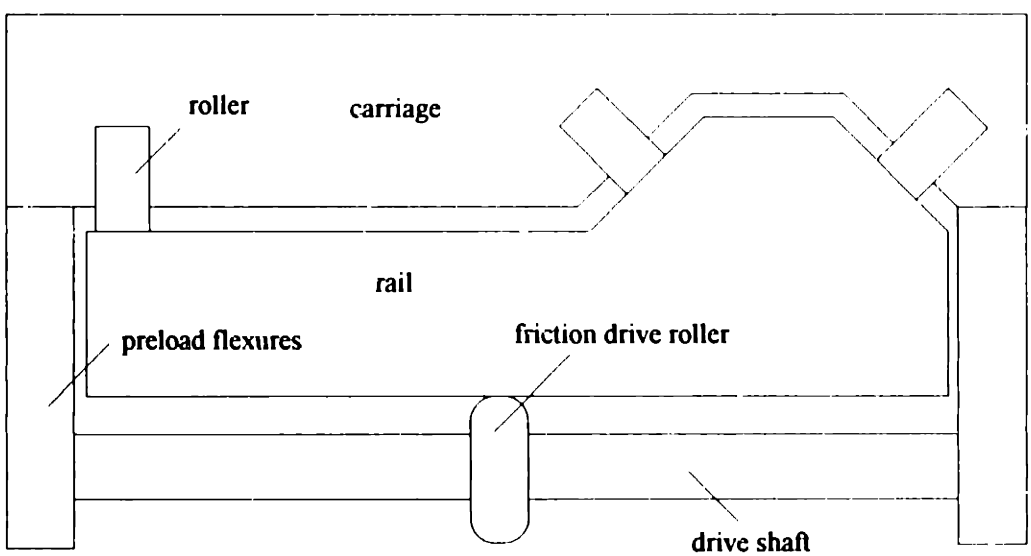

Figure 4.3: A kinematic design for the carriage after [3].

Kinematic Carriage

Figure 4.4: Prototype of a kinematic linear motion system.

A friction drive, which uses the bearing rail itself as the drive bar, provides the driving force and is clamped to the carriage so that it preloads the five bearings. Control of a friction drive can be considerably more difficult than control of a lead screw as discussed later. An alternative is to drive the system with a linear electric motor, where the coils that back the iron's attraction to the magnets would provide the preload force for the five rollers. The rail was made from ceramics. Steel was considered as a more conventional alternative, but was rejected for the reasons outlined below. For example, the cost for a rail with 0.3 μm surface finish and 5 μm overall straightness would exceed the cost for a ceramics rail of same or better specifications.

4.2 Theory

The interface zone for the case of a crowned roller on a flat race is shown in Figure 4.5.

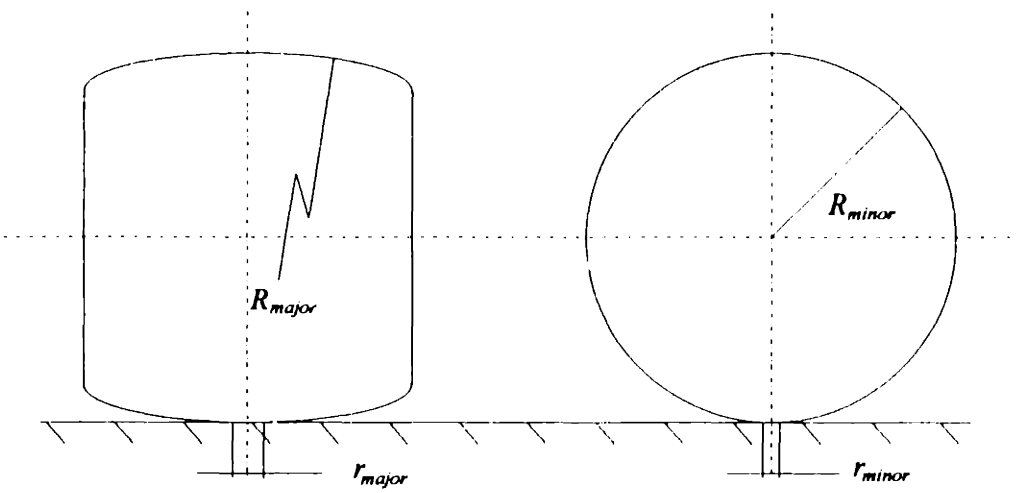

Figure 4.5: Geometry of the contact zone for a roller touching the race.

With $R_{major2} = R_{minor2} = \infty$, $R_{major1} = R_{major}$ and $R_{minor1} = R_{minor}$, the theory as outlined in Chapter 2, Equations 2.4 and 2.7 reduce to:

$$\frac{1}{R_e} = \frac{1}{R_{major}} + \frac{1}{R_{minor}} \tag{4.1}$$

$$\cos(\vartheta) = \frac{R_e}{R_{minor}} - \frac{R_e}{R_{major}} = \frac{R_{major} - R_{minor}}{R_{major} + R_{minor}} \tag{4.2}$$

This transforms the problem to that of a sphere touching a plane as described in Chapter 2. Thus, the calculation of the elliptical contact area and the maximum stress remain the same and will not be repeated here.

4.2.1 Error Motions

As in Chapter 2, the calculation starts with the geometry and the forces. If motion in the X direction is assumed, the X component of Equation 2.1 will give the speed:

$$v_x = \frac{1}{b} \Sigma F_{x,contact} \tag{4.3}$$

with b the coefficient of dynamic friction, here assumed to be the same for all contacts. For the computation it is easiest to assume motion in only one direction, say X. In other cases the coordinate system should be transformed. The calculation precedes in the same way as outlined in Chapter 2, with the only difference that the translational error motion in X direction can be set to zero as a servo drive mechanism will take these errors into account. The spreadsheet in Appendix C, developed by Slocum [3], calculates the error motions and the steady state velocity for the linear motion system, depicted in the assembly drawing in Appendix D.

4.3 Solution

The solution for the study consists of three parts: the rail, the carriage and the motor. It will be explained how the design was made and what factors influenced the decision.

4.3.1 The Rail

The realization of the one degree of freedom resulted in a rail. It had to fulfill three tasks: supporting the carriage, guiding it on a straight line and serving as a bar for the friction drive. From this, the rail has to provide four functional surfaces, Figure 4.6: two forming a vee, one for the flat and one for the friction drive.

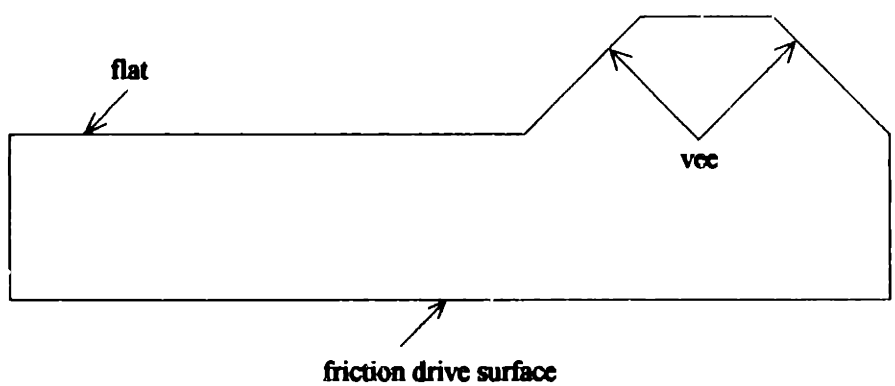

Figure 4.6: Cross-section of the rail with the functional surfaces.

4.3.1.1 Material Selection

It was decided to make the rail from aluminum oxide (alumina). Key issues were toughness and durability, desired qualities at both the carriage interface and the friction drive interface. Cost was another factor in favor of alumina. At the required level of accuracy, the ceramic rail turns out to be less expensive than a hardened stainless steel rail because it is easier to attain high surface finish and straightness in a ceramic rail. Additional desirable properties of the alumina chosen are the dimensional stability and its resistance to water and most chemicals, i.e. an alumina rail will not oxidize or corrode as most metals would. Furthermore ceramics generally do not exhibit micro-corrosion or fretting which is an important factor for dry running systems.

The use of steel rollers as standard parts especially favored ceramics, as the wear behavior becomes deterministic, from the steel roller to the rail. The high surface finish of the alumina makes it act as a micro-fine lap. The surface of the steel rollers improves with use. This gains importance especially in aggressive environments and the absence of lubrication, as in many applications in the chemical industry but also, e.g., in laser copiers.

Maximum stress is the most critical constraint in the design with ceramics. Although plastic deformation is out of question if one looks for high accuracy and high repeatability the absence of a plastic regime will make the part break spontaneously if the critical stress is reached.

For most ceramics the level of allowable stress is higher than that of steel. Higher allowable contact stresses at the carriage interface will yield a higher load capability of the coupling. For alumina this is not the case, the allowable Hertzian

stress of $\sigma_{Alumina} = 1.5E+9\,Nm^{-2}$ is lower than that of hardened steel $\sigma_{Steel,HRC55} = 2.5E+9\,Nm^{-2}$, but in this lightly loaded application this limit was not an issue.

The lack of a plastic regime implies that the state of the part is known exactly. Once machined it will keep its dimensions and if there is no wear, it will not change its physical dimensions. If local overload occurs, it will break or corners will chip off, but the accuracy of the remaining part will have the same dimensional qualities as before. A steel part on the other hand, will indent or bend without clear evidence of the loss of its dimensional stability, and one may not realize it until much later. This is especially important for mass production of precision products. The problems associated with the brittle behavior of ceramics can be overcome with fiber inlays, e.g. silicon carbide whisker reinforcement, or other modern treatments.

The manufacturing of ceramic components has also become easier in recent years. The designer in close cooperation with the materials specialist at the manufacturing site has been given more freedom to specify features such as holes or surface finish. Still the manufacturing process should be kept in mind to avoid excessive costs. The shape should be simple, as the part will eventually be cold isostatically pressed and fired in a kiln. Any functional surface that requires treatment should be easily accessible so that a diamond polishing wheel can contour the surface. Features of low accuracy like counter bores can be machined easily in the green state before firing using carbide tools.

4.3.2 The Carriage

The carriage was built as shown schematically shown in Figure 4.3 and in more detail in the assembly drawing in Appendix D. The carriage has to carry the payload and has to support the rollers, the drive shaft and the motor. If gravity is insufficient to preload the system, additional preload has to be provided, e.g. by a friction drive. The carriage body should be made sufficiently stiff so that it does not deform considerably. Overall performance would be degraded as it would affect the motion of the rollers and the drive mechanism.

The rollers are ABEC 7 precision bearings with crowned outer races made from stainless bearing steel. They are attached to the carriage through shoulder screws which ideally position the rollers perpendicular to the rail. Perfect alignment would give no slip. Reality and cost will result in misalignment and will introduce slip. Slip means that the contact points move relative to the rail, orthogonal to the desired motion. For example, the roller will move away from the ideal trajectory (the straight line) and will do so until a restoring force builds up that may abruptly pull it back to the trajectory, eventually overshooting. This cross-motion happens at a comparatively high velocity that will amplify the surface roughness resulting in an increased Z error motion of the carriage. This is evidenced by the sound that the system makes at high velocity. Thus it is important, that the rollers are aligned carefully and that the direction of the rollers does not change excessively if the system is loaded. Applied loads are the preload and payload to be carried by the carriage. A stiff carriage design will reduce load induced slip. If slip is present, rotational motion is necessary to bring the roller

back to the ideal trajectory. This is easier for crowned outer races with their elliptical contact areas than it is for cylindrical rollers and line contact.

The application discussed herein required additional preload which was achieved by springs that would pull the shaft and with it the friction roller against the rail as shown in Figures 4.7 and 4.8.

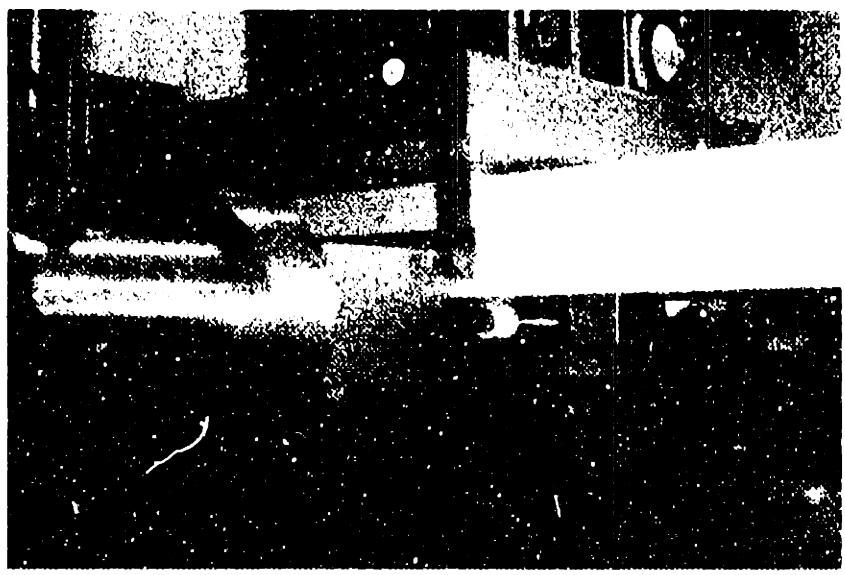

Figure 4.7: Friction drive roller.

The friction drive axial force is transmitted form the carriage to the shaft housing by flexures. The location of the pivot point will determine whether the compliance is increased or decreased by the flexure. This directly affects the behavior of the carriage assembly in the presence of surface roughness. The smaller the stiffness of the flexure-spring combination, the easier the carriage will move over surface errors without affecting preload and hence friction and ultimately the velocity.

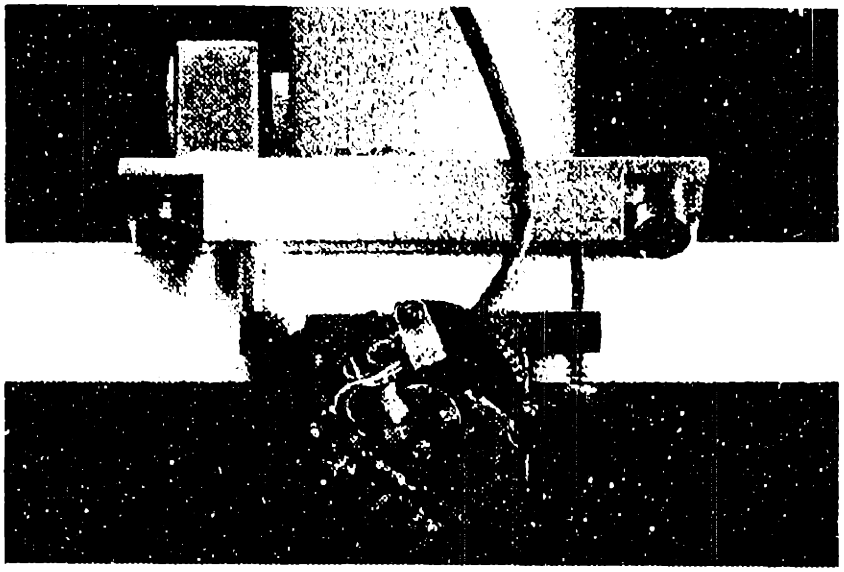

Figure 4.8: Preload mechanism using a flexure and preloaded spring.

If the stiffness is high the preload will vary more and will produce a varying load on the motor. Thus a compromise has to be found that balances ease of motion with demands on the controller of the motor. A linear electric motor preloaded system will have force variations due to electromagnetic discontinuities.

4.3.3 The Motor

A permanent magnet synchronous motor was mounted to the carriage. It was driven from a controller card inside a computer. Initial tests showed immediately that this particular motor would not be able to run the carriage at design speed. To explain the problems and give some background on the motor behavior, its basic characteristics shall be described in some detail along with the modeling assumptions.

The motor is also known as direct current brushless motor because modern power electronics makes permanent magnet synchronous motors behave like dc motors operating without brushes. Permanent magnets are attached to the rotor and the armature windings in the stator are electronically commutated. The stator windings are wound sinusoidally, interrupted by the slots in the cage of the stator. Through this departure from the pure sinusoid the rotor has certain preferred positions that show as 'cogging torque', a torque always being present to a certain degree. The better the sinusoidal approximation can be made, the smaller the cogging torque will be. If the stator windings are skewed, the preferred positions are spread out over larger angles and the impact is reduced. It would be much more difficult to twist the permanent magnets on the rotor. As the rotor will always have an even number of poles, an odd number of slots in the stator will further reduce the amount of cogging.

All these ideas are incorporated in the new motor which is used to drive the friction drive. In addition a new, more flexible controller card is being used and the resolution of the feedback sensor has been more than doubled in the new design. The initial prototype was difficult to control.

The underlying concepts of optimizing the performance of brushless dc motors running at low speed are elaborated in [19] and shall be restated here briefly.

4.3.4 Motor Control

For high performance in controls, feedback to the controller has to be provided, the control loop from output to input has to be closed. This lets the controller

react to the error and correct for it to optimize performance. In our case, and with most modern controllers, the controller is implemented digitally in software.

The gain in flexibility favors the digital implementation, no hardware changes have to be made to change controller algorithms and parameters. The negative aspect of digital control is quantization. To feed the signal into the controller it has to converted from an analog quantity, e.g. position, to a digital, e.g. encoder counts. The output from the controller has to be translated back into analog signals to drive the motor. This translation can only be done in steps, whose size is a function of the analog to digital converters, ADC, and the digital to analog converters, DAC.

4.3.4.1 Quantization

These quantized signals restrict the controller's ability to perform high accuracy control. The quantization can be considered to be noise and the controller needs to filter the signal or reconstruct it. Especially if derivatives of the feedback signals are being used, a simple backward difference scheme for differentiation of the unfiltered signals will give highly polluted values, unacceptable for high performance control algorithms. These problems are amplified in the case, where the resolution of the desired quantities is insufficient. For example, the resolution of the velocity δ_v calculated from a position feedback signal quantized at δ_x and a fixed sampling time T:

$$\delta_v = \delta\left(\frac{dx}{dt}\right) = \frac{\delta_x}{T} \tag{4.4}$$

The velocity resolution must be higher than the required accuracy. For example, a position resolution of 0.5 μm and a sampling time of 1 ms will yield a velocity resolution of 0.5 mms^{-1}. If the design speed was 3 mms^{-1} then errors smaller than about 16% cannot be detected. The velocity resolution can be increased by either reducing the absolute resolution of the feedback position sensor or by increasing the sampling time, where the former increases costs while the latter reduces the bandwidth of the controller, i.e. its ability to react promptly to disturbances.

4.3.4.2 Observer

The need to filter noise polluted feedback signals and to recover the information they contain leads to high performance filters, known also as observers or estimators.

The observer takes the feedback signal as input and computes estimates of it and, if desired estimates of derivatives of it and of other immeasurable quantities. The controller consequently takes these estimates as input and calculates the output, in our case the signals to the power-electronics that drive the motor.

Hence it operates on the best approximations of the physical analog quantities available.

4.3.4.3 Motor Model

How well the observer performs depends on the model employed. The more accurate the model, the better the observer will predict the physical quantities. Large efforts are typically spent to obtain more accurate models, as exact

predictions translate in many cases directly into cost savings. For a slow running dc brushless motor, this means to derive the non-linear mathematical description that describes how currents, voltages, flux densities and torques are related, reduce them in order by Park-like state transformations to a set of still non-linear equations, and eventually linearize them around an operation point, where possible.

4.4 Measurements

For the measurements, a prototype of the linear motion system was built. It consists of the kinematic carriage traveling on an alumina rail, a dc brushless motor with the power-electronics and the feedback sensors, and the controller. Straightness and position were measured with a laser interferometer. The hardware and software interfaces were established and programs for the data-analysis were written.

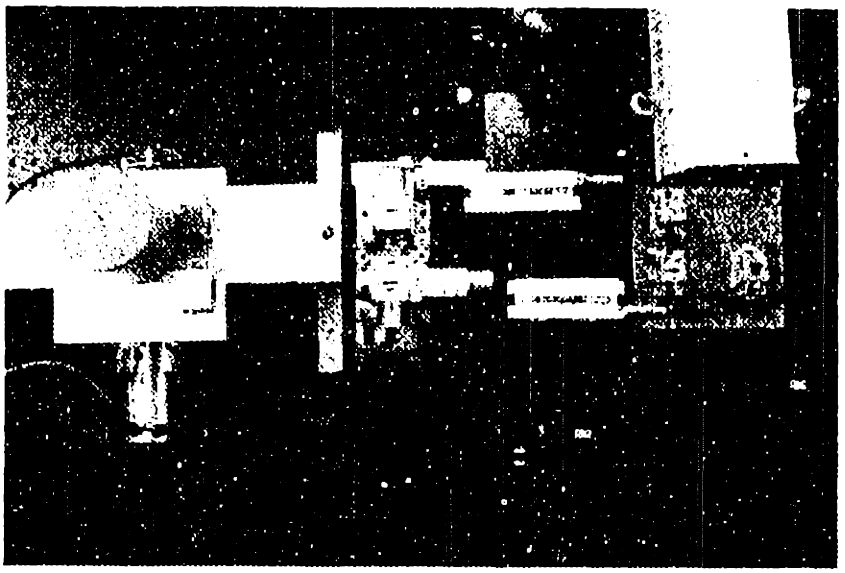

Figure 4.9: The laser paths for X and Z position measurement.

A ZYGO AXIOM 2/20 laser interferometer was set up so that the beam was parallel to the rail as shown in Figure 4.9.

At one end of the rail a differential plane mirror interferometer (DPMI) was set up, at the other end the straightness mirror was fixed. The laser beam was split in order to take two measurements: X and Z position. The moving optics, prism and retroflector were installed on the carriage. The optics were carefully aligned and fixed with hot glue, which has the advantage of fixing without applying forces that could result in misalignment. Details on alignment and considerations on how to set up a laser interferometer measurement system can be found in [20].

The straightness measured in this test setup is the straightness as experienced by the top plate of the carriage. This straightness will be a function of the rail and the carriage. The measurement procedure relies strongly on a smooth and slow motion. Otherwise, noise pollutes the data, real features may be hidden and

artificial problems may develop. Even though the motor initially could not perform to design specifications, for the straightness measurements the motion was slow and smooth enough.

The measurements were analyzed in the frequency domain. The gathered data were transformed by a discrete spatial (fast) Fourier transform [21, 22, 23]. They were displayed as spectral component over wavelength which corresponds to the length of period in the case of the temporal Fourier transform. This way periodic errors (and only those) and the distance between marks caused by them show very clearly.

4.4.1 Rail Measurements

The measurements on the rail showed an overall bow of about 10 μm. A spectral decomposition of the error shows that the short wavelength spectral components of the error stay below 0.25 μm, as shown in Figures 4.10 and 4.11.

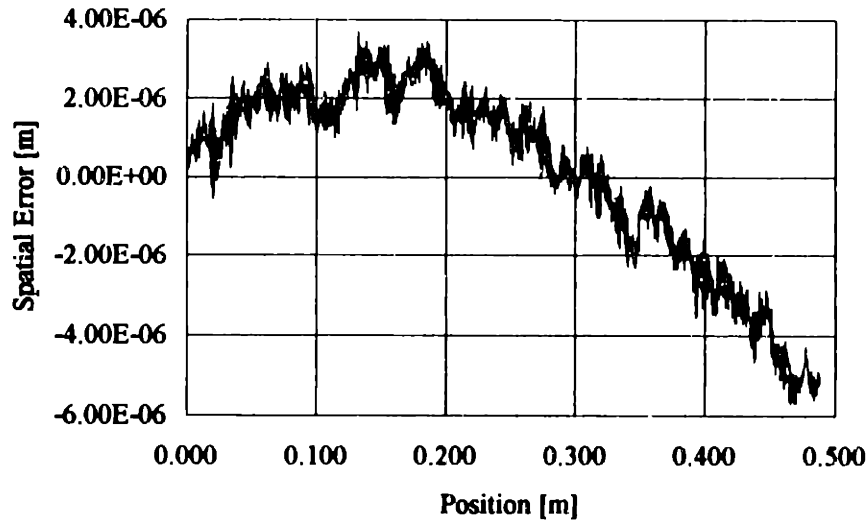

Figure 4.10: The straightness error of the moving carriage.

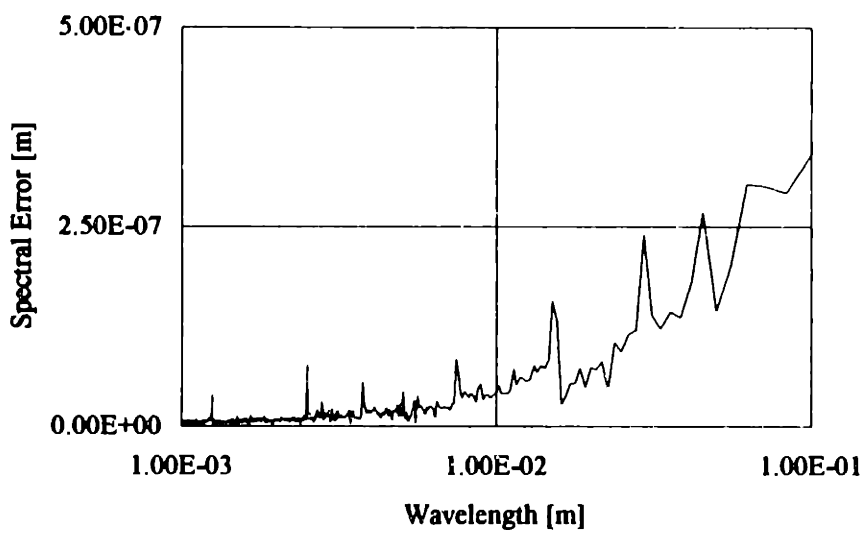

Figure 4.11: The spectral components of the carriage's straightness error.

Due to the limited resolution of the measurement procedure, wavelengths shorter than 1 mm could not be captured. However the contact area between the roller and the rail is of the order of millimeters, effectively averaging over errors of smaller wavelengths. Furthermore the data in Figure 4.11 indicates that the errors decrease with decreasing wavelength. Figures 4.12 and 4.13 show data of a single trace from a ZYGO MAXIM 3D surface profilometer. The 3D picture showed the expected surface features such as negative skewness or holes that will eventually fill up with particles and make the surface appear smoother. This feature is perhaps best described as self-lapping. Note that the overall bow of the ZYGO data is only about 1 μm. The difference to the measurements in Figure 4.10 can be explained by the fact that the ZYGO measurement procedure measures the straightness of the rail itself and not the straightness of the carriage. The remaining straightness error must be due to the rollers and other noise sources like slip and the effects of the friction drive roller.

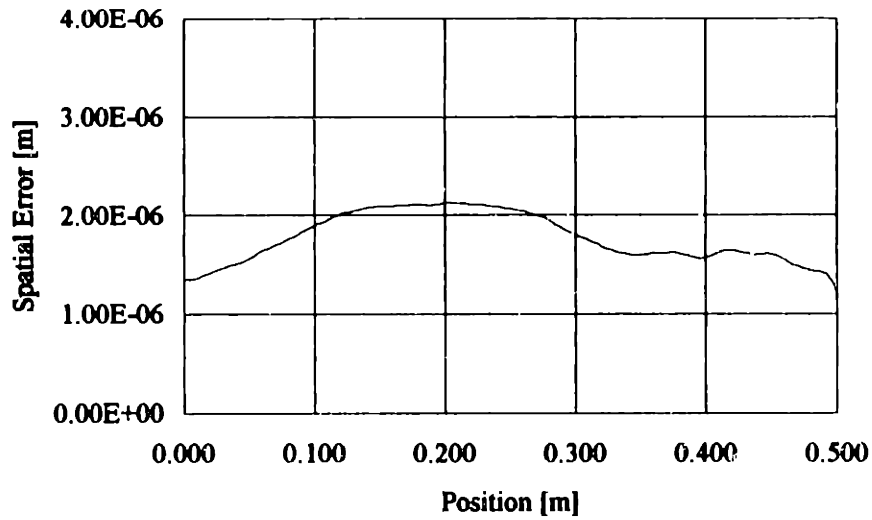

Figure 4.12: The surface profile of the rail (ZYGO MAXIM 3D).

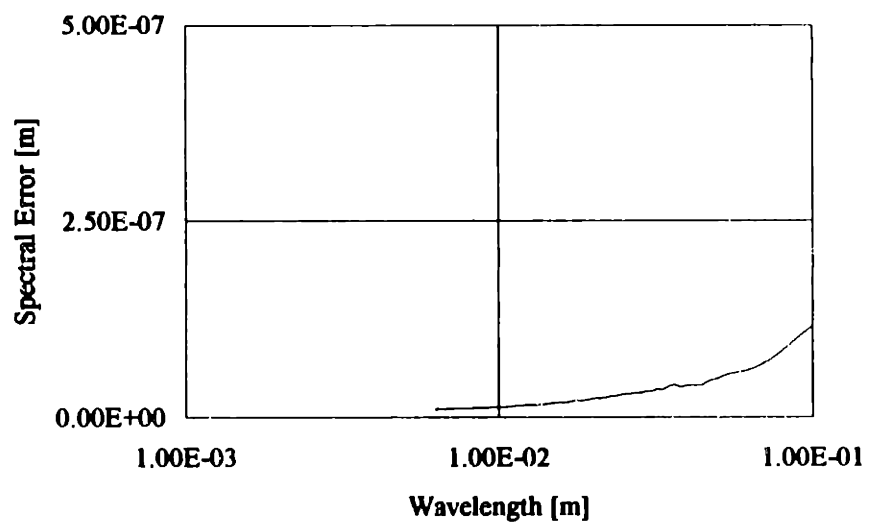

Figure 4.13: The rail's spectral error components (ZYGO MAXIM 3D).

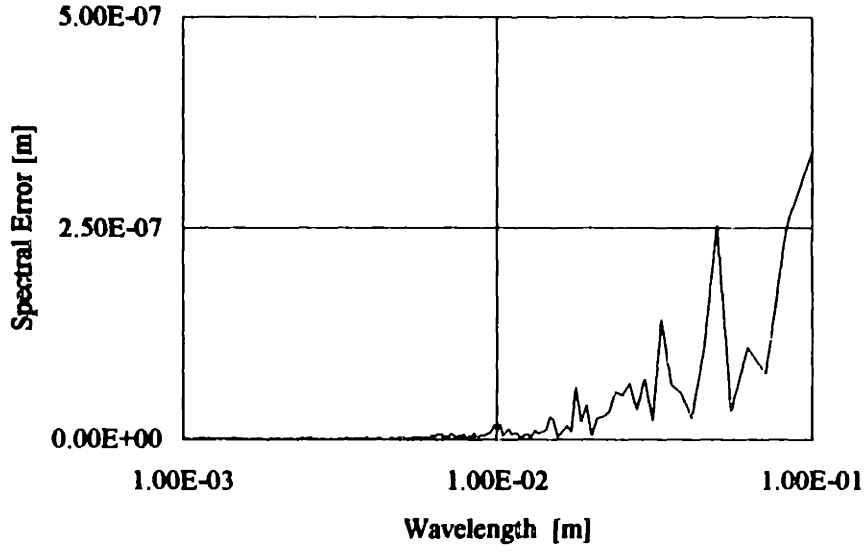

Figure 4.14: Measurement noise of the carriage's straightness measurements.

Figure 4.14 shows the background noise, the data were taken with the carriage at rest. This data will serve as reference for the straightness measurements. It shows that the level of noise reaches 0.25 μm at wavelengths larger than 30 mm. These data are important when interpreting the other test results.

To show the wear behavior of the stainless steel rollers on the ceramics rail, a wear test was conducted. Figures 4.15 and 4.16 show the straightness after 500 and 110,000 cycles. From this data it can be concluded that wear does not affect the straightness in a detrimental manner. Wear occurs only at the contact of the rail and the friction roller. This is partly due to the rough surface of the ground bottom. It has be noticed that a ground ceramic surface has sub-surface damage (cracks) that reduce its allowable contact stress drastically. Lapping removes these effects.

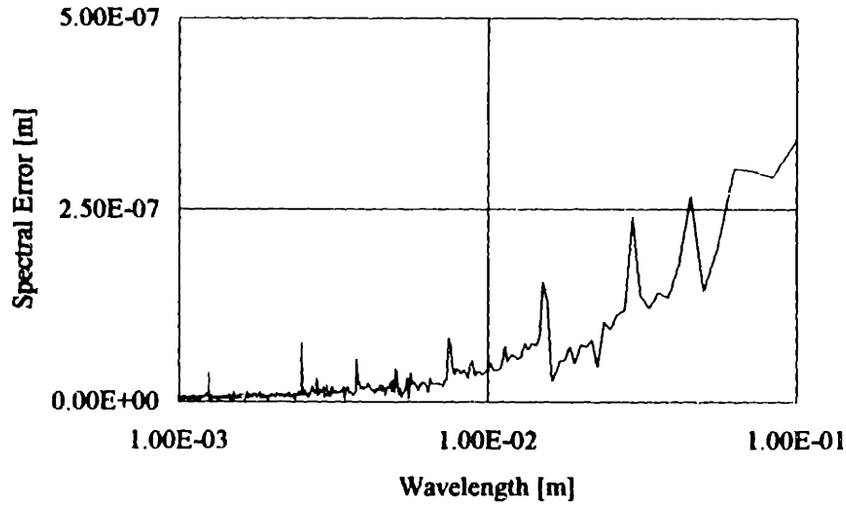

Figure 4.15: Carriage straightness of the rail after 500 cycles.

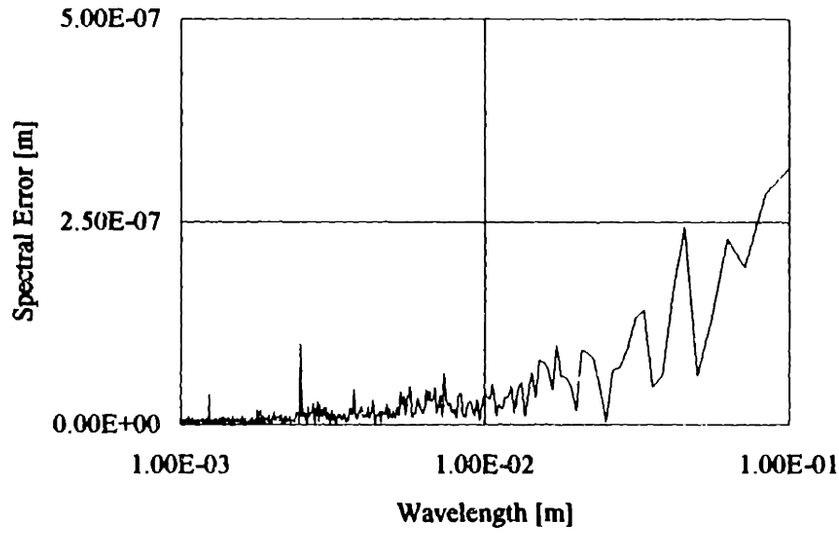

Figure 4.16: Carriage straightness of the rail after 110,000 cycles.

After about one hundred cycles a thin black streak with metal particles would form on the rail where it contacts the steel rollers. This showed the wear of the rollers into the rail, most likely due to the oxidation particles filling up the micro-valleys in the ceramic rail surface. Around the metal particles a zone of lighter wear would form. Evidently the carriage was rolling over these particles, not touching the race at these points. The particles would stay for about two thousand contacts with a roller before being worn away. An effect of these particles on the effective surface roughness could not be measured.

The width of the streak was measured to be 2 mm, which the analysis confirmed as the right order of magnitude of the contact area for the roller touching the flat race.

4.4.2 Drive Measurements

Tests at a speed eight times design speed still showed a very large, strongly periodic, error of the order of 7%, Figure 4.17. From a spectral analysis, Figure 4.18, it was concluded that most of the problems are due to the low performance of the motor, especially the high cogging torque.

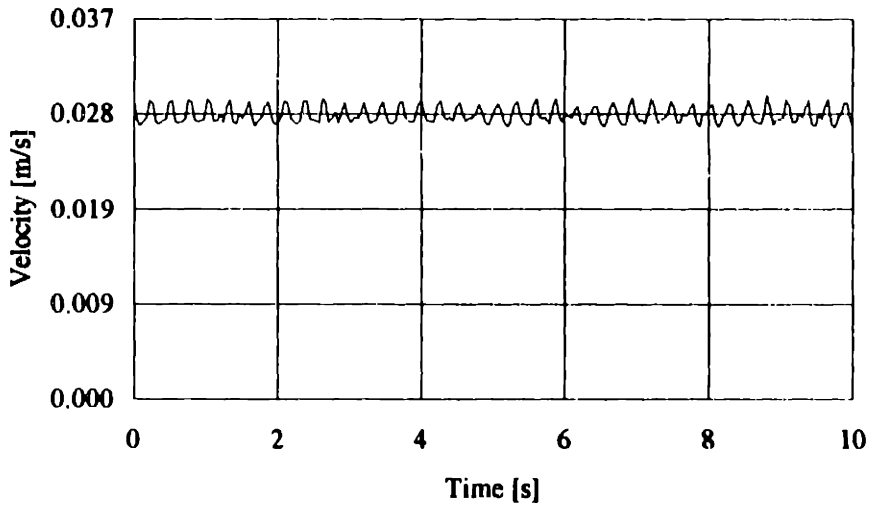

Figure 4.17: The velocity error.

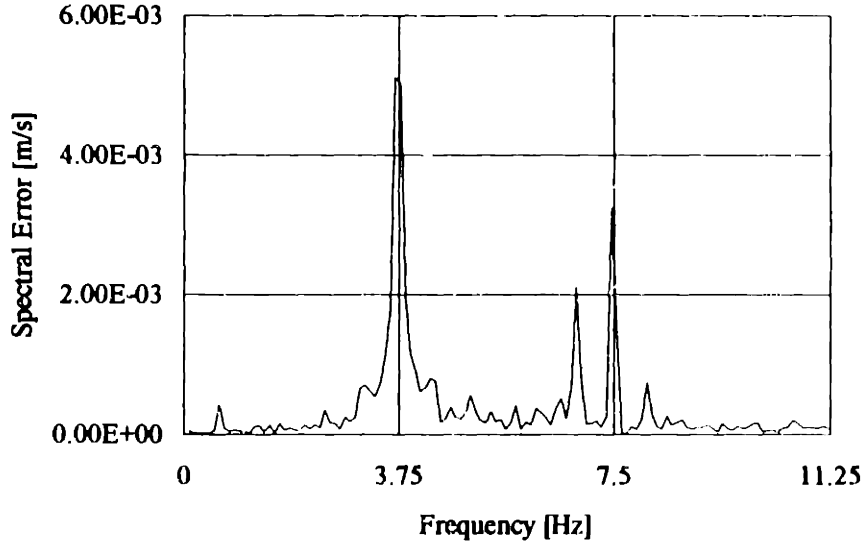

Figure 4.18: The spectral velocity error.

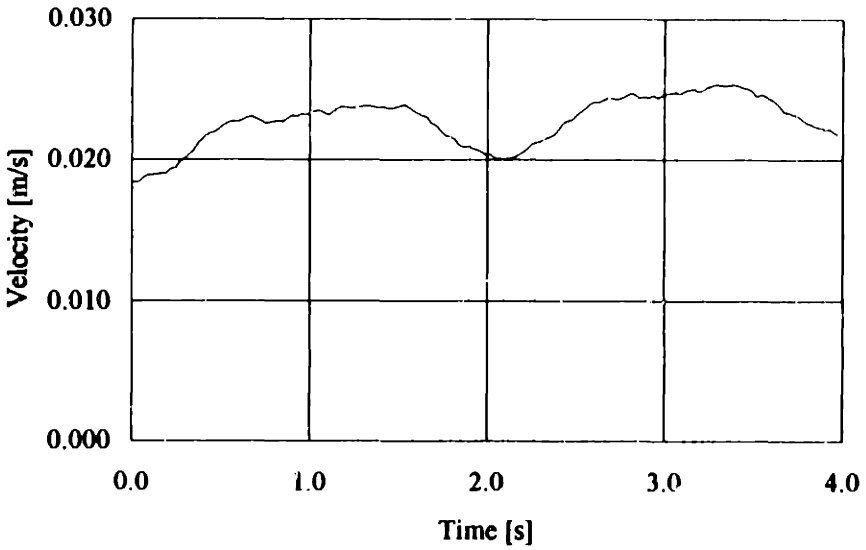

Figure 4.19: The open loop velocity error of the new motor.

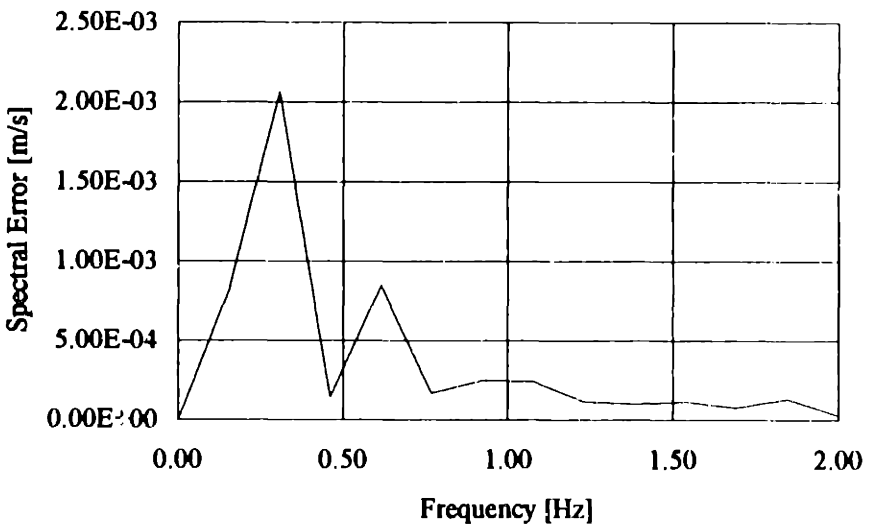

Figure 4.20: The spectral velocity error of the new motor driven open loop.

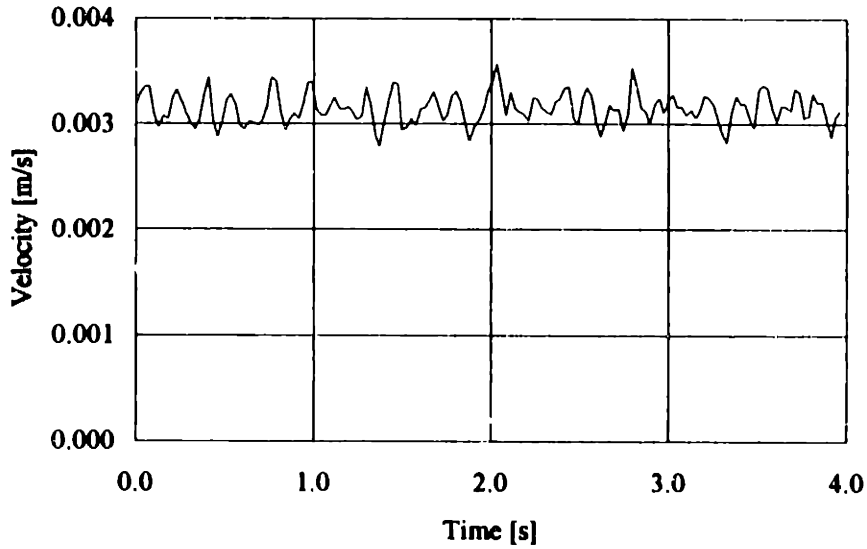

Figure 4.21: The closed loop velocity error of the new motor.

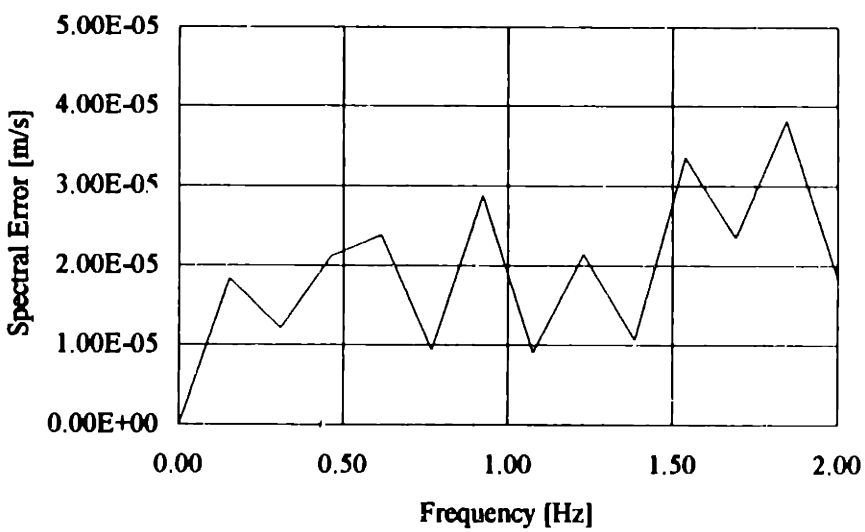

Figure 4.22: The spectral velocity error of the new motor driven closed loop.

The new motor with the features described in Section 4.3.3, showed a smaller error even if driven open loop, Figure 4.19. The spectral decomposition in Figure 4.20 shows two distinct peaks at 0.3 and 0.6 Hz, which corresponds to 1/rev and 2/rev. These could be associated with mechanical inaccuracies, that occur every revolution and electrical inaccuracies, that, through the two pole pairs occur twice per revolution.

If the motor was driven closed loop with PI control on the reconstructed signals from the observer, the carriage could be driven at design speed and the error reduced to about 5% of the nominal speed, Figure 4.21. The error spectrum, Figure 4.22, reveals that the peaks are now within the noise floor, which is about two orders of magnitude lower than the original peaks were.

4.5 Conclusions

The kinematic variation of the linear guide system proved to achieve the desired performance in terms of accuracy, long-term stability and wear. The introduction of ceramics works did not cause major problems. Designing with ceramics requires re-design in some aspects to account for the different manufacturing process. The advantages are in the material properties:

- No brinelling or hardening during operation,
- Potentially no detrimental wear,
- Linear elastic behavior occurs up to very close to the maximum stress,
- High dimensional stability.

In particular, this last point yields a higher performance of the rail and the linear motion system over the whole life time. The dimensional stability can turn out to be a key factor for the use of ceramics, as no other material gives this reassurance of quality.

The motor control is still to be optimized to drive the motor with the specifications. New control algorithms and mapping will help to decrease the velocity error even further.

5. Conclusions

The general concept of kinematic design offers many ways to improve existing designs. It also helps to stimulate the development of new, innovative and cost-effective designs.

The positive aspects are the simplification of the calculation. Dividing the system under consideration into rigid bodies and elastic/plastic contact zones allows the designer to break the calculation into global force computation and local deflection calculation. How these local error motions are combined to give the global error motion of the coupling is explained in detail in Section 2.7. With this simple straightforward calculation, the chances are high that designers will not rely on intuition, expertise, experience and hope to get accurate estimates of design performance.

It could be shown that the stability of a kinematic system can be easily evaluated by means of linear algebra. This check is based on the condition number [4]. Compared to previously employed, graphically and semi-empirically methods, [3, 6], the stability is clarified and more easily evaluated.

Kinematic design, which is statically determinate, reduces assembly costs. The position of kinematically jointed members to each other does not depend on accurate, expensive alignment but it is guaranteed by the design and produces no cost. This inexpensive gain in assembled accuracy and repeatability will especially benefit consumer products and high volume products, where, due to the high costs lower accuracy solutions are often employed.

The negative aspects are the high contact stresses inherent to truly kinematic designs. One way to increase the load capacity is to use quasi-kinematic

arrangements and design for finite contact regions, another is to employ materials that can withstand high contact stresses. With new materials kinematic design can advance into areas where the properties of conventional materials have excluded it until recently.

6. Recommendations for Future Research

The next important step is to verify the analytical performance prediction by building and testing the kinematic coupling designed in Chapter 3 and given in Appendix B. With the experimental results, the analysis and calculations could be refined where necessary and effects of the surface finish could be assessed more comprehensively.

The calculation of the coupling error motions should be extended to allow the designer to specify all angles arbitrarily. Even though symmetry can save costs and computational time, sometimes required specialized stiffness distributions could request the angles to be specified arbitrarily. A further enhancement to the calculations would be to include an option for line and finite area contact as opposed to point contact. This would enable the computation to handle both kinematic and quasi-kinematic designs.

In the current design of the kinematic linear motion system, changes should be made so that the position of both the support rollers and the friction roller with respect to the carriage and the rail would be kinematic and thus would not require alignment. Any misalignment in the rollers will cause slip and will reduce the performance of the system.

The calculations of the error motions of the linear motion system could be enhanced to calculate the deflections from Hertzian contact theory.

It is also recommended to compare different types of ceramic materials with respect to their repeatability/cost performance. This would provide the designer

with a wider range of possible material combinations and would allow him to match his requirements more closely.

Most important of all is the search for new and old applications where kinematic design or re-design could increase the performance.

7. References

[1], C. Evans: **Precision Engineering: An Evolutionary View,** Cranfield University Press, 1989.

[2], W. Beitz, W. Pahl: **Methodisches Konstruieren**, Springer, 1988.

[3], A. Slocum: **Precision Machine Design,** Prentice Hall, 1991.

[4], W. H. Press et. al.: **Numerical Recipes (FORTRAN Version),** Cambridge University Press, 1989.

[5], A. Donmez, A. Slocum: **"Kinematic Couplings for Precision Fixturing, Part II"**, Journal of Precision Engineering, Vol. 10, No. 3, July 1988.

[6], J. C. Maxwell: **"General Considerations Concerning Scientific Apparatus"**, The Scientific Papers of J. C. Maxwell, Vol. II, Cambridge University Press, London, 1890.

[7], R. S. Ball: **A Treatise on the Theory of Screws,** Cambridge University Press, London, 1900.

[8], H. Hertz: **Über die Berührung fester elastischer Körper**, Journal für reine und angewandte Mathematik, Barth, 1881.

[9], W. Beitz, K.-H. Küttner: **Dubbel, Taschenbuch des Maschinenbaus,** Springer, 1988.

[10], I. Szabó: **Höhere Technische Mechanik,** Springer, 1953.

[11], The MathWorks Inc.: **MATLAB User Guide**, Prentice Hall, 1990.

[12], P. Schmiechen: **"Theory and Computation of Kinematic Couplings"**, to be published, 1992.

[13], Ernst Abbé: **"Meßapparate für Physiker"**, Zeitschrift für Instrumentenkunde, Vol. 10, 1890.

[14], M. Weck: **Werkzeugmaschinen,** VDI, 1990.

[15], P. Schmiechen: **"A Kinematic Tool Holder Coupling"**, Term project report for the Precision Machine Design class at MIT, 1992.

[16], A. Slocum: **"Design of a Three Groove Kinematic Coupling"**, Journal of Precision Engineering, April 1992, Vol. 14, No 2.

[17], A. Donmez, A. Slocum: **"Kinematic Couplings for Precision Fixturing, Part I"**, Journal of Precision Engineering, Vol. 10, No. 2, April 1988.

[18], L. Hale: **"A Spreadsheet based Design Tool for Three Teeth Kinematic Couplings"**, Term project report for a tribology class at MIT, 1992.

[19], F. Bhathena: **Precision Low-Speed Digital Control of a Permanent Magnet Synchronous Motor**, Master's thesis in Electrical Engineering, MIT, 1993.

[20], Anonymous: **Axiom 2/20 Laser Measurement System, Operation and Reference Manual**, ZYGO, 1991.

[21], D. E. Newland: **Random Vibrations and Spectral Analysis**, Wiley, 1984.

[22], R. B. Randall: **Frequency Analysis**, Bruel and Kjaer, 1987.

[23], A. G. Piersol, J. S. Bendat: **Random Data: Analysis and Measurement**, Wiley, 1986.

8. Appendices

8.1 Appendix A: Spreadsheets for the Kinematic Coupling

Kinematic Coupling Design Spreadsheet

Last modified: 4/5/1992

Coupling geometry data

XY plane is assumed to contain the ball centers.

For standard coupling designs, contact forces are inclined at 45 to the XY plane.

Standard 120 degree equal size groove coupling? **TRUE**

For non standard designs, enter geometry after results section.

Dball =	**0.008**	Ball diameter
Rgroove =	**-0.0048**	Groove radius (negative for a trough)
Dcoupling =	**0.044**	Coupling diameter
Fpreload =	**-500**	Preload force over each ball
Extend =	**0.052**	Distance from coupling center
Rotation =	**0.000**	Rotation around Z axis
Xerr =	**0.000**	X location of error reporting
Yerr =	**0.052**	Y location of error reporting
Zerr =	**0.000**	Z location of error reporting

Auto select material values assume that metric units are used (mks)

Ball/Groove = **4** 1: (SiN/SiN); 2: (SiN/Ala); 3: (SiN/RC62 Fe);
4: (RC62 Fe/RC62 Fe); 5: other

Applied forces' Z,Y,Z values & coordinates Coupling centroid

FLx =	**10.00**	XL =	**0.000** xc	0.000
FLy =	**10.00**	YL =	**0.052** yc	0.000
FLz =	**20.00**	ZL =	**0.000** zc	0.000

Results:

Error motions at the reporting point

	Fixed	Rotating		Fixed
DeltaX	**2.59E-07**	**2.59E-07**	EpsX	**1.28E-05**
DeltaY	**8.79E-08**	**8.79E-08**	EpsY	**7.93E-09**
DeltaZ	**8.49E-07**	**8.49E-07**	EpsZ	**-3.21E-06**

Effective Stiffness (N/micron)

Fx/dx	**39**
Fy/dy	**114**
Fz/dz	**24**

Homogenous Transformation Matrix: for the Coupling Centroid

1.00E+00	**3.21E-06**	**7.93E-09**	**9.21E-08**
-3.21E-06	**1.00E+00**	**-1.28E-05**	**8.79E-08**
-7.93E-09	**1.28E-05**	**1.00E+00**	**1.83E-07**
0.00E+00	**0.00E+00**	**0.00E+00**	**1.00E+00**

Ball-Groove 1

Groove normal forces		*Contact stress*		*Stress/Allow*	*Deflection (+into ball)*	
Fbnone	**3.37E+02**	sigone	**2.59E+09**	**0.71**	delone	**2.98E-07**
Fbntwo	**3.16E+02**	sigtwo	**2.53E+09**	**0.70**	deltwo	**6.72E-07**

Ball-Groove 2

Groove normal forces		*Contact stress*			*Deflection*	
Fbnthree	**3.67E+02**	sigthree	**2.66E+09**	**0.73**	delthree	**-2.41E-07**
Fbnfour	**3.53E+02**	sigfour	**2.63E+09**	**0.72**	delfour	**1.54E-08**

Ball-Groove 3

Groove normal forces		*Contact stress*			*Deflection*	
Fbnfive	**3.59E+02**	sigfive	**2.64E+09**	**0.73**	delfive	**-9.81E-08**
Fbnsix	**3.61E+02**	sigsix	**2.65E+09**	**0.73**	delsix	**-1.29E-07**

Generic data entry for non-120 degree couplings

The coupling is assumed to lie in the XY plane.

Enter X,Y,Z coordinates and alpha, beta, gamma direction cosines for Ball 1

	Contact point 1		Contact point 2
Xba =	**0.002828**	Xbb =	**-0.002828**
Yba =	**0.022000**	Ybb =	**0.022000**
Zba =	**-0.002828**	Zbb =	**-0.002828**
Aba =	**-0.707107**	Abb =	**0.707107**
Bba =	**0.000000**	Bbb =	**0.000000**
Gba =	**0.707107**	Gbb =	**0.707107**

Enter characteristics for groove 1 and ball 1

Egone =	**2.04E+11**	Groove material elastic modulus
vgone =	**0.29**	Groove material Poisson ratio
Rgone =	**-0.0048**	Groove radius of curvature
Ebone =	**2.04E+11**	Ball material elastic modulus
vbone =	**0.29**	Ball material Poisson ratio
Dbone =	**0.008**	Ball diameter
Sone =	**3.62E+09**	Allowable Hertz stress

Enter preload forces' X,Y,Z components and coordinates

Fpxone =	**0**	Fpxtwo =	**0**	Fpxthree =	**0**
Fpyone =	**0**	Fpytwo =	**0**	Fpythree =	**0**
Fpzone =	**-500**	Fpztwo =	**-500**	Fpzthree =	**-500**
Xpone =	**0**	Xptwo =	**-0.019053**	Xpthree =	**0.019053**
Ypone =	**0.022**	Yptwo =	**-0.011**	Ypthree =	**-0.011**
Zpone =	**0.016**	Zptwo =	**0.016**	Zpthree =	**0.016**

Calculations:

Build Force Moment equilibrium matrices: AF = B (Equations 1-6)

Matrix A

Fbn1	Fbn2	Fbn3	Fbn4	Fbn5	Fbn6
-7.07E-01	7.07E-01	3.54E-01	-3.54E-01	3.54E-01	-3.54E-01
0.00E+00	0.00E+00	-6.12E-01	6.12E-01	6.12E-01	-6.12E-01
7.07E-01	7.07E-01	7.07E-01	7.07E-01	7.07E-01	7.07E-01
1.56E-02	1.56E-02	-7.78E-03	-7.78E-03	-7.78E-03	-7.78E-03
0.00E+00	0.00E+00	1.35E-02	1.35E-02	-1.35E-02	-1.35E-02
1.56E-02	-1.56E-02	1.56E-02	-1.56E-02	1.56E-02	-1.56E-02

B with loads	B w/o loads	F with applied loads		F with preload only	
-1.00E+01	0.00E+00	fbnone	336.84	fone	353.55
-1.00E+01	0.00E+00	fbntwo	316.27	ftwo	353.55
1.48E+03	1.50E+03	fbnthree	367.28	fthree	353.55
-1.04E+00	0.00E+00	fbnfour	352.69	ffour	353.55
0.00E+00	0.00E+00	fbnfive	359.11	ffive	353.55
5.20E-01	0.00E+00	fbnsix	360.85	fsix	353.55

Original ball corrdinates

xboneO	0.0000000	xbtwoO	-0.0190526	xbthreeO	0.0190526
yboneO	0.0220000	ybtwoO	-0.0110000	ybthreeO	-0.0110000
zboneO	0.0000000	zbtwoO	0.0000000	zbthreeO	0.0000000

New ball coordinates (=original + ball deflection*direction cosines)

xboneN	0.0000001	xbtwoN	-0.0190526	xbthreeN	0.0190526
yboneN	0.0220000	ybtwoN	-0.0109999	ybthreeN	-0.0110000
zboneN	0.0000003	zbtwoN	-0.0000001	zbthreeN	-0.0000001

Ball centers' deflections

dxone	1.32E-07	dxtwo	-4.53E-08	dxthree	5.40E-09
dyone	0.00E+00	dytwo	7.85E-08	dythree	9.35E-09
dzone	3.43E-07	dztwo	-7.98E-08	dzthree	-8.01E-08

Theory applicability check:

Initial dist. between balls		Final dist. between balls		Difference	
LotI	0.038105	LotN	0.038105	DLotI	-2.07E-08
LttI	0.038105	LttN	0.038105	DLttI	-5.07E-08
LtoI	0.038105	LtoN	0.038105	DLtoI	7.14E-08

Change in length/distance between balls	Deflection/ball radius	Ratio (should be >5)
5.43E-07	1.68E-04	3.09E+02
1.33E-06	6.03E-05	4.53E+01
1.87E-06	3.21E-05	1.71E+01

Coupling centroid is assumed to be at intersection of coupling triangle's angle bisectors

Initial centroid		Distance ball to centroid		Error motion at centroid	
xci	0.00E+00	Dcone	2.20E-02	dxc	9.21E-08
yci	-3.47E-18	Dctwo	2.20E-02	dyc	8.79E-08
zci	0.00E+00	Dcthree	2.20E-02	dzc	1.83E-07

Original angles between balls			Original altitude lengths		
Angone	60.0000	angle ball 1	Aone	0.0330	Ball 1 to side 2 3
Angtwo	60.0000	angle ball 2	Atwo	0.0330	Ball 2 to side 1 3
Angthree	60.0000	angle ball 3	Athree	0.0330	Ball 3 to side 2 1

New angles between balls			Original sides' angle with X axis		
AngoneN	60.0001	angle ball 1	Aot	60	Side opposite ball 3
AngtwoN	59.9998	angle ball 2	Att	0	Side opposite ball 1
AngthreeN	60.0001	angle ball 3	Ato	120	Side opposite ball 2

New sides' angle with X axis			
AotN	59.9997	Side opposite ball 3	0
AttN	-0.0001	Side opposite ball 1	0
AtoN	119.9998	Side opposite ball 2	

Original altitudes' slope angles and Y intercepts			
AmtwoO	30	AbtwoO	-3.4694E-18
AmthreeO	150	AbthreeO	-3.4694E-18

Rotation about opposite side (radians)

Ttt	1.04E-05	rotation about side 23 due to Z motion at ball 1
Ttc	-2.42E-06	rotation about side 13 due to Z motion at ball 2
Tot	-2.43E-06	rotation about side 12 due to Z motion at ball 3

Coupling error rotations

EpsX	1.28E-05	EpsZ1	-6.00E-06	Z rot from ball 1
EpsY	7.93E-09	EpsZ2	-4.12E-06	Z rot from ball 2
EpsZ	-3.21E-06	EpsZ3	4.91E-07	Z rot from ball 3

8.2 Appendix B: Mechanical Drawings of the Kinematic Coupling

Bottom Part

Scale 1 : 1

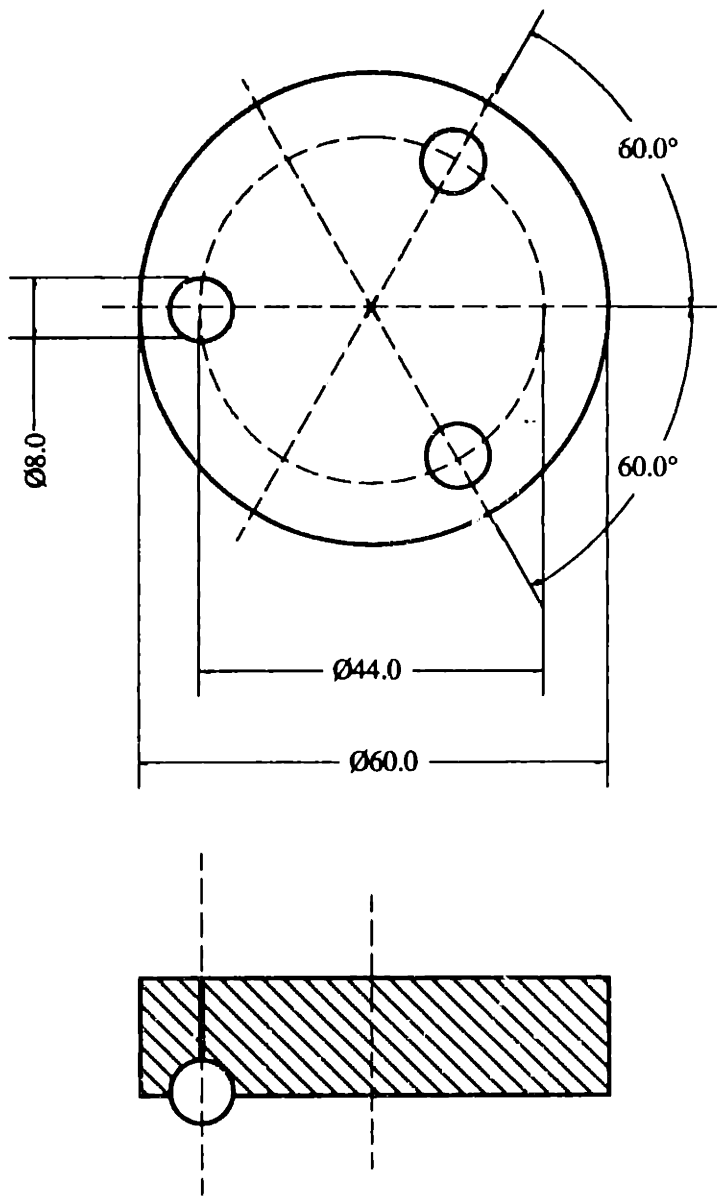

Any further features (holes, etc.): > 8mm away from the contact points!

Top Part

Scale 1 : 1

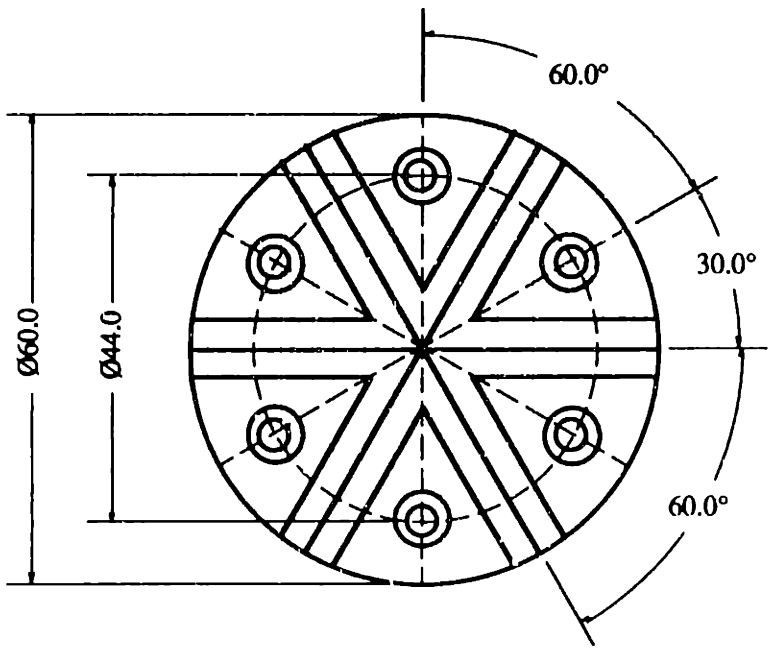

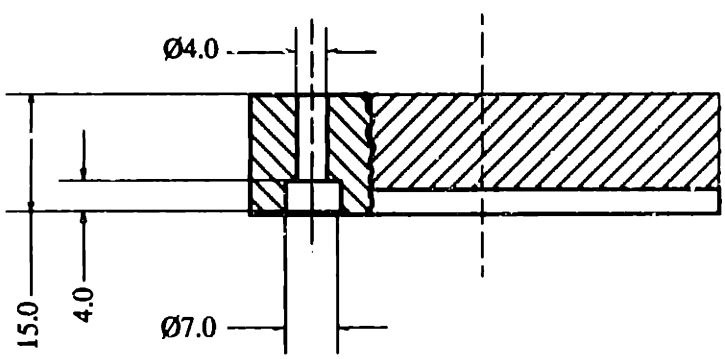

Any further features (holes, etc.): > 8mm away from the contact points!

Detail of the Coupling Interface

Scale 2 : 1

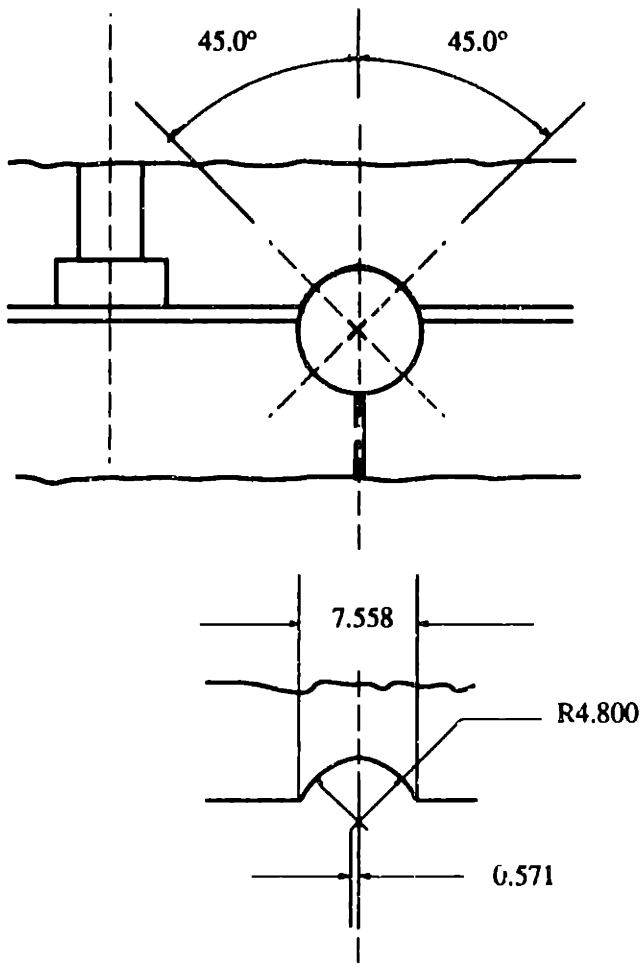

Around the contact points: Surface finish: Ra = 0.1 micrometer, hardened HRC 62

NO CHAMFER !
KEINE FASE !

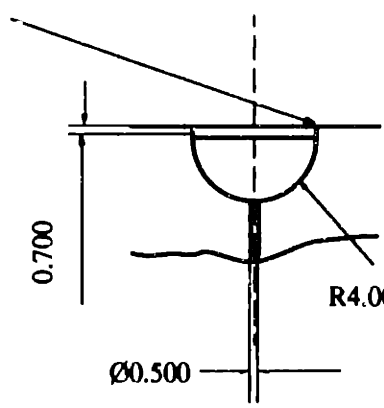

To match balls 8 mm Tungsten Carbide

8.3 Appendix C: Spreadsheets for the Kinematic Carriage

Kinbear.xls
Analysis of errors in a inematically supported carriage

Enter numbers in bold

Desired steady state velocity		**0**		
Contact point 1 coordinates, direction cosines, stiffness, friction coef.				
xb1	**0.000**	alph1	**0.000**	
yb1	**0.000**	beta1	**-0.707**	lower left .
zb1	**-0.253**	gama1	**0.707**	
Kb1	**100000**			
ms1:	**0**	md1:	**0.005**	static and dynamic friction
ma1	**1**			
mb1	**0**			
mg1	**0**			
Contact point 2 coordinates, direction cosines, stiffness, friction coef.				
xb2	**0.000**	alph2	**0.000**	
yb2	**0.000**	beta2	**-0.707**	upper left
zb2	**0.253**	gama2	**-0.707**	
Kb2	**100000**			
ms2:	**0**	md2:	**0.005**	
ma2	**1**			
mb2	**0**			
mg2	**0**			
Contact point 3 coordinates, direction cosines, stiffness, friction coef.				
xb3	**6.000**	alph3	**0.000**	
yb3	**0.000**	beta3	**-0.707**	lower right
zb3	**0.253**	gama3	**-0.707**	
Kb3	**100000**			
ms3:	**0**	md3:	**0.005**	
ma3	**1**			
mb3	**0**			
mg3	**0**			

Contact point 4 coordinates, direction cosines, stiffness, friction coef.

xb4	6.000	alph4	0.000	
yb4	0.000	beta4	-0.707	upper right
zb4	-0.253	gama4	0.707	
Kb4	100000			
ms4:	0	md4:	0.005	
ma4	1			
mb4	0			
mg4	0			

Contact point 5 coordinates, direction cosines, stiffness, friction coef.

xb5	3.000	alph5	0.000	
yb5	0.000	beta5	-1.000	flat
zb5	3.500	gama5	0.000	
Kb5	100000			
ms5:	0	md5:	0.005	
ma5	1			
mb5	0			
mg5	0			

Applied forces (up to three) and locations. Fx1=vx*(md1+md2+md3+md4+md5)

Ffx1	100	Ffx2	0	Ffx3	0
Ffy1	500	Ffy2	500	Ffy3	500
Ffz1	0	Ffz2	0	Ffz3	0
xf1	3	xf2	0	xf3	0
yf1	3	yf2	0	yf3	0
zf1	3	zf2	0	zf3	0

Applied torques

Gam x	0
Gamy	0
Gamz	0

Determine the bearing point reaction forces from [A]{F}={S}

	vx	F1	F2	F3	F4	F5	Sum
Sum Fx	-0.025	0.000	0.000	0.000	0.000	0.000	-100
Sum Fy	0.000	-0.707	-0.707	-0.707	-0.707	-1.000	-1500
Sum Fz	0.000	0.707	-0.707	-0.707	0.707	0.000	0
Sum Mx	0.000	-0.179	0.179	0.179	-0.179	3.500	1500
Sum My	0.000	0.000	0.000	4.243	-4.243	0.000	-300
Sum Mz	0.000	0.000	0.000	-4.243	-4.243	-3.000	-1200

Results: Steady state velocity and bearing reaction forces

vx	4000	**Bearing deflections**	
f1b	732	d1b	7.32E-03
f2b	803	d2b	8.03E-03
f3b	-45	d3b	-4.55E-04
f4b	25	d4b	2.53E-04
f5b	429	d5b	4.29E-03

New coordinates of bearings in carriage reference frame:

Bearing 1		**Bearing 2**		**Bearing 3**	
xb1n	0.0000000	xb2n	0.0000000	xb3n	6.0000000
yb1n	0.0051786	yb2n	0.0051786	yb3n	-0.0003214
zb1n	-0.2585536	zb2n	0.2590536	zb3n	0.2530536

Bearing 4		**Bearing 5**	
xb4n	6.0000000	xb5n	3.0000000
yb4n	0.0001786	yb5n	0.0042857
zb4n	-0.2535536	zb5n	3.5000000

Error motions (microunits)		**HTM**				
ex	-270.42		1	-0.00179	-0.000125	0.00E+00
ey	-125.01		0.0017917	1	0.00027042	-1.06E-02
ez	1791.68		0.000125	-0.00027	1	-3.19E-04
			0	0	0	1.00E+00
dy	-10607.21					
dz	-318.58					

8.4 Appendix D: Assembly Drawing for the Kinematic Carriage